

Statement of independent work

I hereby declare that this thesis has been carried out independently and in agreement with "Forskrift om krav til mastergrad" established by the Norwegian Ministry of Education and Research, 01.12.2005, and in agreement with supplementary regulations concerning Master theses at the Norwegian University of Science and Technology (NTNU).

Abstract

The solvation structures of the divalent cations of Mg, Ca, Sr and Cu in water at infinite dilution are investigated using QMSTAT. In this approach the investigated system is divided into three interacting parts; The central QM-region consisting of a single ion, a discrete solvent region consisting of 100 water molecules described with the NEMO force field and a dielectric continuum surrounding the system. The discrete water molecules act as a perturbation to the Hamiltonian in the QM-region, including effects from electrostatics, polarizabilities and an exchange repulsion term calculated from the overlap between orbitals on water and the ion.

The report aims, for the first time to test QMSTAT with divalent ions and thus the strongest intermolecular forces ever investigated using this method. The goal is to determine the coordination structure of the ions mentioned, an area where there still is disagreements regarding the coordination number and the distance from the ion to the oxygens of water.

For Mg^{2+} we observe a coordination number, CN of 6 all through the simulations and a first peak in the Mg-O radial distribution function, $r_{\text{Mg-O}} = 2.12 \text{ \AA}$. For Ca^{2+} , we get an CN alternating between 6 and 8, $r_{\text{Ca-O}} = 2.50 \text{ \AA}$. For Cu^{2+} we get a CN of 6 in an elongated octahedral structure with $r_{\text{Cu-O},1} = 1.96$ and $r_{\text{Cu-O},2} = 2.45 \text{ \AA}$. For Sr we get an alternating CN between 7 and 8 with $r_{\text{Cu-O},2} = 2.60 \text{ \AA}$. These results are in agreement with previous QM/MM simulations and are within the uncertainty limits of experimental results. Simulations performed using one week of CPU time using QMSTAT have given similar results to QM/MM simulations requiring one year.

It has also been tested to reproduce the near-IR spectrum of Cu^{2+} in water. This was not successful, but despite of this it is believed that the coordination structures obtained are reliable.

*Den som har hovudet over vatnet,
ser berre toppen av isfjellet*

Contents

1	Introduction	1
2	Experimental methods	3
2.1	Neutron diffraction	3
2.2	XANES and EXAFS	4
2.3	Ligand Field Theory and NIR	4
3	Computational methods	6
3.1	Born-Oppenheimer	7
3.2	Slater determinants	7
3.3	Self Consistent Field	8
3.4	Basis sets	8
3.5	Monte Carlo simulations	9
3.6	Molecular Dynamics	10
3.7	QM/MM	11
3.8	MOLCAS	12
3.9	QMSTAT	15
3.10	Float chart for the calculations	22
4	Previous results	23
4.1	The hydration of Mg^{2+}	23
4.2	The hydration of Ca^{2+}	23
4.3	The hydration of Sr^{2+}	24
4.4	The hydration of Cu^{2+}	24
5	Computational details	26
5.1	Supermolecular calculations	26
5.2	Simulations	27
5.3	Data Analysis	30
6	Results	32
6.1	Supermolecular calculations	32
6.2	QMSTAT potentials	36

6.3	Simulations	44
7	Discussion	61
7.1	Quality of the results	61
7.2	The coordination of Mg^{2+}	61
7.3	The coordination of Ca^{2+}	62
7.4	The coordination of Sr^{2+}	62
7.5	The coordination of Cu^{2+}	62
7.6	The absorption spectrum of Cu^{2+}	63
7.7	The QMSTAT approach	63
8	Conclusion	67

Chapter 1

Introduction

When we look at a glass of water, it seems as if we are watching a persistent, unchanging continuum where not much is happening. If we put a nail of iron in the water, it takes days, even weeks before we can see signs of rust. When adding salt, the process is somewhat faster, but the reaction is still so slow that we do not have the patience to follow it. If we take a much closer look at the glass, we see a more lively substance. Zooming in so that we can see the single atoms of water, ions from the salt and from the rusting nail will also be visible, all tightly surrounded by water molecules. The picture is neither as persistent as it seemed from a distance. 10^{10} times every second, the water molecules closest to the ions of iron leave, letting other water molecules take their places [1]. For every such exchange, the hydrogen bonds, keeping the water molecules together, break and reform one hundred times [2]. Even in that, almost non-existing time interval, the hydrogen atom, covalently bond to oxygen, has vibrated back and forth another hundred times [3].

This illustrates one of the large difficulties in computational chemistry. We want to describe processes that take seconds, days and even years, while still taking into account the effects happening on the subpicosecond scale. PJ van Maaren proudly proclaimed his foresight for the computational chemistry: *Microsecond, here I come!* By that, illustrating the fact that simulations in computational chemistry are still not capable of lasting longer than this. This project aims to bring us one tiny step forward toward the understanding of coordination chemistry with the help of a method based solely on Quantum Mechanics.

To understand how ions behave in water is an important problem, yet often poorly understood. We know that positive ions are surrounded by water molecules with oxygen facing the positive charge, but in many cases the certain knowledge stops there. We only have estimates to the number of water molecules surrounding the solvated ion and to how far away they are [1]. Since all chemical reactions require a proximity between the reactive species, reactions in water demand the removal of water from the inner coordination sphere for both the reactants involved [4].

If one wants to understand liquid reaction chemistry, it is indeed interesting to know the answers to questions like: How many waters surround the iron ion in hemoglobin and how much free energy is required to remove one of these to give room for an oxygen molecule? When a calcium ion moves between neurons, how many water molecules surround it and slow down the neural signal? And why can cobaltous chloride solved in water be used as an invisible ink?

It is here important to note that even monatomic ions are not only soft spheres with a charge, but can possess asymmetries and large polarizabilities. For higher order metal ions, e.g. the transition metals, the partially filled *d*-orbitals give rise to directional changes in charge density around the ion. When water molecules, with its strong dipoles, approach these ions, some directions are more attractive than others, thus some configurations become more stable than others. The water molecules can also polarize the ions and induce asymmetries in the charge distribution.

Coordination chemistry can also be seen as a step on the way to understanding enzyme-catalyzed processes. Often an enzyme-catalyzed reaction takes place near a metal ion, without which, the enzyme would be inactive. The enzyme changes the electronic structure of the ion which again acts as the direct catalyst. The polypeptide backbone of the enzymes ensures the proximity of the ion and the reactive species, but does not by itself have any significant catalytic function [5].

To learn more about coordination chemistry one can perform experiments or do computer simulations. We have chosen the latter strategy and have simulated a set of divalent cations in water using a new procedure called QMSTAT [6] which will be described in detail later. The procedure has not yet been tested on many different systems and this is the first time it will be tested with divalent ions, meaning also the strongest intermolecular forces tested. This project thus have two main goals. To determine the coordination structure of a set of ions in water and to test whether the QMSTAT approach can be used to investigate such systems. To understand the significance of the results we start by introducing some general experimental and computational methods used to determine the coordination structure of ions.

Chapter 2

Experimental methods

The most common experimental procedures used to elucidate the coordination of ions in water make use of diffraction in some sort, either neutrons diffracting with the cores surrounding the ion or electromagnetic radiation interacting with the electronic clouds of the surrounding molecules. An important fact with these methods is that they measure an absorption or emission over a range of time. No information of processes that happen on a shorter time scale than the characteristic vibration of the method will be gained [7]. To illustrate this, the characteristic timescale of some experimental methods are given in table 2.1 together with the time required for some of the processes that we want to investigate.

Table 2.1: Characteristic time scales for processes in solution and experimental methods

Timescale	Processes	Experimental methods
10^{-14}s	Hydrogen vibrations	Femtosecond laser
10^{-13}s	Vibration of heavier elements	
10^{-12}s	Hydrogen bonds break and reform	IR
10^{-11}s		IR
10^{-10}s	Exchange of waters in the first coordination shell of metal ions	IR
10^{-9}s		NMR, XANES
10^{-8}s		NMR, XANES
10^{-7}s		NMR, XANES
10^{-6}s	Longest MD simulations so far	NMR, XANES

2.1 Neutron diffraction

A neutron diffraction experiment uses a neutron source (e.g. a nuclear reactor) and let a ray of neutrons diffract with a sample. Because neutrons are

uncharged they do not interfere with the electron clouds in molecules, only with the cores. Neutron diffraction experiments thus give information regarding the positions of the cores. It gives good information about the radial distribution function described in section 5.3.1. A problem is that for ions in solution neutron diffraction experiments required until recently very concentrated solutions, for copper, more than 1 molar of CuX_2 had to be used, X is a soft counter-ion e.g. NO_3^- or ClO_4^- [8]. Pure water contains 55 moles of water per liter. This means that 55 water molecules should solvate three ions. The proximity of other ions will here inevitably lead to disturbance of the measured data and differ from computational data, which mostly describe a system at infinite dilution. Neutron Diffraction methods used to study water chemistry have been reviewed by Marcus [9].

2.2 XANES and EXAFS

XANES is an acronym for X-ray Absorption Near Edge Spectrum and EXAFS for Extended X-ray Absorption Fine Structure. They are, as the names, used interchangeably in the literature imply, X-ray methods for determining the structure of a molecule. The absorption lies in the keV range and is the result of excitation of core electrons ($1s$, sometimes $2s$ for heavy elements) up to unoccupied p -orbitals. The edge in question is the sudden onset of absorption when the energy of the X-rays overcome the excitation energy barrier, and the interesting part of the spectrum is not the edge itself, but the region close (± 50 eV) to it, which gives information regarding the environment of the excited specie. This specie will radiate electromagnetic radiation that will be scattered from atoms close to it. It is possible to calculate a XANES spectrum given a structure and this can be taken as a negative test as to whether the structure is present in a sample or not. On the other hand, it is not straightforward to calculate a structure given a XANES spectrum. To perform these kind of experiments, high energy radiation is required and this is usually provided from a synchrotron. The method has been reviewed by Lee et al. [10].

2.3 Ligand Field Theory and NIR

The copper ion in water is traditionally seen as a classical example of the Jahn-Teller effect [11]. The ion has the electronic structure $[\text{Ar}]d^9$ with one singly occupied d -orbital. We look at what happens when Cu^{2+} is placed in an octahedral field with six negative charges on the x , y and z axes representing six ligands, e.g. the oxygen atoms of water. The two d -orbitals $d_{x^2-y^2}$ and d_{z^2} pointing toward the axes will be degenerate and higher in energy than the three degenerate orbitals pointing between the axes, d_{xy} , d_{xz} and d_{yz} . The Jahn-Teller theorem [12] then states that:

Any non-linear molecular system in a degenerate electronic state will be unstable and will undergo distortion to form a system of lower symmetry and lower energy, thereby removing the degeneracy

Since we have two degenerate states, with either $d_{x^2-y^2}$ or d_{z^2} being singly occupied, the complex will undergo a distortion to remove this degeneracy. There are at least two ways to accomplish this, see figure 2.1. One is to move the two water molecules along the z axis further away and bring the waters in the xy -plane closer. This will lead to the d_{z^2} being lower in energy and the hole in the d -orbitals will be located in the xy -plane. On the other hand, one may equally well bring the two waters along the z -axis closer and let the other four move further away. This would lead to the opposite situation and the hole would be located in d_{z^2} . The traditional picture of copper is the first one with four close and two more distant waters (4+2).

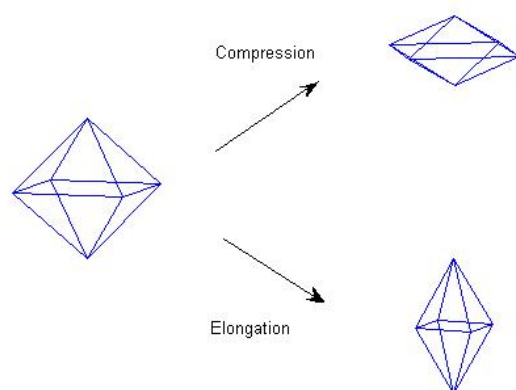


Figure 2.1: The two possible Jahn Teller distortions of $[\text{Cu}(\text{H}_2\text{O})_6]^{2+}$.

Near Infrared-spectroscopy (NIR) gives information of this ligand field splitting by exciting one electron from a fully occupied d -orbital to the singly occupied one. The electron can be excited from any of the four doubly occupied d -orbitals and the degree of splitting is a measure of the environment of the ion. NIR has been thoroughly described in the book by Siesler et al. [13].

Chapter 3

Computational methods

Since the 1920's, the rules that govern all chemical processes are known. The laws of quantum mechanics and relativity had both been formulated and the Dirac equation [14] was able to combine these theories. These laws are formulated as differential equations, and in the following we will be considering the non-relativistic time independent Schrödinger Equation [15]:

$$H\Psi_i(r_\nu, r_j) = E_i\Psi_i(r_\nu, r_j) \quad (3.1)$$

This eigenvalue equation can be solved to give a set of possible eigenstates or wavefunctions, Ψ_i of a system depending on the coordinates of the nuclei r_ν and the electrons r_j . The system is described by the Hamilton operator H and the eigenvalues E_i of the equation are the energies of the corresponding eigenstates. Further significance of the different terms in equation 3.1 can be found in any introductory text to quantum mechanics, e.g. [16]. For a set of nuclei and electrons the Hamiltonian will in atomic units take the form

$$H = \frac{1}{2}\nabla_\nu^2 + \frac{1}{2}\nabla_i^2 + \sum_{i<j} \frac{1}{r_{ij}} + \sum_{\nu<\mu} \frac{q_\nu q_\mu}{r_{\nu\mu}} + \sum_{\nu,i} \frac{q_\nu}{r_{\nu i}} + V_{ext}. \quad (3.2)$$

The Greek indices ν and μ denote nuclei and i and j electrons. The first term is the kinetic energy of the nuclei and the second of the electrons. The three next terms are the electrostatic interaction energy, electron-electron, nucleus-nucleus and nucleus-electron respectively. The last term is an external field that might be present. Equation 3.1 can only in a few cases be solved exactly and in the following some approximations and numerical methods to solve it will be presented.

3.1 Born-Oppenheimer

The lightest nucleus, that of hydrogen is 2,000 times heavier than an electron. One consequence of this, is that the electrons will be changing position much more rapidly than what the nuclei will do. This is exploited in most quantum mechanical calculations by applying the Born-Oppenheimer approximation [17]. Here it is assumed that when the nuclei change positions, the electrons will immediately redistribute to adapt to the new field. Then the Hamiltonian can be written as a sum of two terms, one for the electrons where the position of the nuclei is only included parametrically, and one for the nuclei which move classically in the field of the electrons. If the Hamiltonian can be written as such a sum, where each term is only dependent on one set of coordinates then the wave functions can be written as a product where each factor contains only one of these sets [11]. In this case the nuclear wave function and the electronic;

$$\Psi(r_\nu, r_i) = \Psi_{el}(r_i; r_\nu)\Psi_n(r_\nu), \quad (3.3)$$

the semicolon indicating that the electronic wave function depends on the position of the nuclei parametrically. $\Psi_{el}(r_i; r_\nu)$ is the electronic wave function and solves the equation

$$H_{el}(r_\nu)\Psi_{el}(r_i; r_\nu) = E_{el}(r_\nu)\Psi_{el}(r_i; r_\nu). \quad (3.4)$$

Where E_{el} describes how the electronic energy of the system changes with the position of the nuclei. The repulsion and kinetic energy of the positive nuclei are added to give the total energy.

3.2 Slater determinants

In computational chemistry the spatial extension and spin of an electron is usually represented in a spin orbital, or a one electron wave function, $\chi(r, m_s)$. The simplest way to create a molecular wave function from a set of spin orbitals is to form the Hartree product, the direct product of the spin orbitals:

$$\Psi_{Hartree}(\mathbf{r}) = \chi_1(r_1, m_{s1})\chi_2(r_2, m_{s2}) \cdots \chi_n(r_n, m_{sn}) \quad (3.5)$$

One of the problems with the Hartree product is that it does not satisfy the Pauli principle [11]. The wave function does not change sign under interchange of two electrons, it is not antisymmetric. There exists a simple way to write all linear combinations of Hartree products that give an antisymmetric wave function. This is done with the now famous Slater determinant:

$$\Psi(\mathbf{r}) = \frac{1}{\sqrt{n!}} \begin{vmatrix} \chi_1(r_1) & \chi_2(r_1) & \cdots & \chi_n(r_1) \\ \chi_1(r_2) & \chi_2(r_2) & \cdots & \vdots \\ \vdots & \vdots & \ddots & \vdots \\ \chi_1(r_n) & \cdots & \cdots & \chi_n(r_n) \end{vmatrix} \quad (3.6)$$

It can be seen that interchanging the labels of two of the electrons corresponds to interchanging two rows in a determinant, which leads to a change of sign. If the spinorbitals are orthonormal, the Slater determinant will be normalized by the prefactor.

3.3 Self Consistent Field

Self Consistent Field (SCF), also termed Hartree-Fock [18] is, because of its simplicity and intuitive interpretation the most used quantum chemical method, at least as a starting point for calculations. We start by noting that if the wave function of a system containing N electrons was known, then we would know the electric field in all points in space of the system. If we then were to put another electron into this system, we can assume that it would move in the average field of the N electrons and we could solve the Schrödinger equation for it. Of course, this new electron would change the environment of the other electrons and their wave function would alter to adapt to the new man in town. SCF works along these lines of thinking. First an initial guess is made for all the spin orbitals except for one. The wave function for the last one is found by solving the Schrödinger Equation in the field of the other electrons. Then another orbital is chosen and a new wave function is calculated for this orbital in the field of all the other electrons. This procedure is repeated until convergence. The thing that SCF neglects is that the electrons interact instantaneously. In real systems these charge fluctuations will be correlated to lower the total energy of the system and more sophisticated quantum chemical methods include more and more of this correlation and are expected to be improvements to SCF.

3.4 Basis sets

The spin orbitals are in practical calculations almost always described as linear combinations of a set of basis functions.

$$\chi = \sum_{i=1}^N c_i \phi_i \quad (3.7)$$

Finding the true solution under a given set of approximations would in general require $N = \infty$ in equation 3.7. What we do, when only using a finite basis, is to find the projection of the true solution into the space spanned by $\{\phi_i\}$. The

quality and amount of these basis functions ϕ_i can to a large degree influence the result. The most widely used basis functions are centered on the nuclei (x_o, y_o, z_o) of the molecular system and are of a Gaussian type first introduced by Boys in 1950 [19]:

$$\phi = (x - x_o)^k (y - y_o)^l (z - z_o)^m e^{-\alpha(r-r_o)^2}, \quad (3.8)$$

where $r^2 = x^2 + y^2 + z^2$. If the sum $k + l + m$ equals zero, we term the orbital *s*-type, if one, *p*-type and so on, following the scheme for terming atomic orbitals by angular momentum quantum numbers. The reason for using Gaussians is that the product of two of them is just another Gaussian, meaning that the analytical evaluation of the integrals is simplified compared to the more physical correct $e^{-\alpha|r-r_o|}$ [11]. In quantum chemical calculations a rule of thumb is that the quality of the results can be improved in two ways: By improving the quantum chemical method or by increasing the basis set. In the SCF method we can improve our results by increasing the basis sets, but we can never avoid the fact that we neglect electron correlation. Thus there is a limit called the Hartree-Fock limit that we can never beat without including this effect. Then we have to use methods that include electron correlation to improve the results. To obtain the best results the improvement in basis sets and the improvement of the QM-method should be made simultaneously.

In this work we name the basis sets after the number of basis functions they contain. E.g. the basis set *7s6p3d2f* contains seven basis functions of *s*-type, six of *p*-type and so on. The α -coefficients for the basis functions can be found in the respective references.

3.5 Monte Carlo simulations

For a system in equilibrium, the probability of being in a given state does not change with time. If we had an ensemble of copies of this system, the fraction of systems being in a given state would equal the time fraction any single system would spend in the same state in the limit $t \rightarrow \infty$. This is called the ergodic hypothesis. This means that a change in state from *A* to *B* occurs exactly as often as a change from *B* to *A*. Let ρ_A and ρ_B be the probability of the system being in state *A* and *B* respectively and π_{AB} be the probability of a transition from state *A* to *B*, given that the system is in state *A*. Then, because of microscopical reversibility the following relation must hold:

$$\rho_A \pi_{AB} = \rho_B \pi_{BA} \quad (3.9)$$

That is, the system goes from state *A* to state *B* exactly as often as the reverse transition. Since the probability of being in a given state at equilibrium is proportional to its Boltzmann factor [20], the ratio between the two transitions can be written as

$$\frac{\pi_{AB}}{\pi_{BA}} = e^{-\beta(U_B - U_A)} \quad (3.10)$$

where U is the potential energy, β equals $(k_b T)^{-1}$ and k_b is the Boltzmann constant. A sampling from a Boltzmann ensemble can be achieved by first taking a random move in phase space, the move is always accepted if it leads to a state of lower energy and accepted with a probability equal to the right hand side of equation 3.10 if the new energy is higher. This scheme is called the Metropolis scheme and was first introduced by Metropolis et al. in 1953 [21]. Simulations done using this method are called Monte-Carlo (MC) simulations after the famous Casino in the wealthiest of Monaco's four quarters, because of their random nature.

An advantage with a Monte Carlo simulation is that there is no need for calculating energy gradients. Only the energy of each sampled configuration is needed when performing the simulation. An obvious disadvantage, is that no time exists in these simulations. Every step is taken in a random direction, thus no realistic trajectories are found, and only the average values have a physical meaning, not the sequence of incidents.

When performing MC-simulations where only pair potentials are involved, it is common to move only one particle in each time step. This way the interaction energy between the rest of the particles remains the same and only the energy of the moved particle has to be recalculated in each step. In our simulation, we include polarizability on all the water molecules and the ability for the central ion to adopt its electronic structure as a response to a changed environment. This way all particles interact through what is called many body effects and we lose the advantage in moving only one particle at a time. Because of this, instead of moving only one particle, all particles are moved in each MC-step, but of course they are moved shorter distances than what would have been the case if only one particle was moved, otherwise nearly every step would have been rejected because of a too high increase in energy. The same configurations would still have been sampled, but the dynamics would have been much slower.

3.6 Molecular Dynamics

The most common way to simulate larger molecular systems is by using classical Molecular Dynamics (MD) [20]. In an MD simulation the forces between atoms are treated classically with particles moving on a potential surface with the motion of the particles governed by Newton's laws of Mechanics. A central aspect in these simulations is the force field. It describes how the simulated energy changes when the atoms in the system move. One of the most widely used is the AMBER force field [22] which is parameterized for a large amount of different molecules. The energy in a force field is usually a function of intramolecular bond lengths and bond angles in addition to pair potentials between atoms on different atoms. The forces that act upon the atoms are the gradients of this potential. The reason why these methods are termed classical, is because, as long as the potential surface is known, the particles are moved according to

classical mechanics. The motion of the electrons is not considered and thus, no quantum mechanics is needed, except for the parameterization of the force field. When the forces have been determined, the atoms are moved in accordance with some integrator which is usually a poor differential equation solver, e.g. the Verlet Velocity Algorithm [23]. It is poor in the sense that it does not solve the differential equations of motion exactly, but it is often fast and since we are usually only interested in the average properties of the system, not exact trajectories, such an integrator can be fully qualified for its purpose. An MD simulation is usually utilized when the gradients are available. It has the advantage that time exists and trajectories can be meaningful. One problem is that since the particles move on a potential surface, the energy of the system remains constant. We are usually however, interested in the properties of a system where the temperature is constant. An MD simulation can sample from a constant temperature ensemble with the use of a thermostat, e.g. Berendsen [24] or Nose-Hoover [25].

3.7 QM/MM

Even though the tools for treating atomic systems with quantum mechanical methods are available, their computational cost make them unfeasible to use for *simulating* molecular systems containing more than 50 atoms in the foreseeable future. One approach to solve large systems with special regions of interest is to use hybrid methods. The interesting part is treated with Quantum Mechanics while the surrounding areas are described using classical Molecular Mechanics, e.g. MD. Such methods are called Quantum Mechanical/Molecular Mechanical methods, QM/MM. Reviews on the subject includes [26] and [27]. There are different approaches to the problem, but a short summary of the main features are described here. The system is first partitioned into a QM-region and a classical region, and often an attempt is made to have a smooth transition phase between the two, through which molecules are allowed to pass. The QM-region is solved with standard quantum mechanical methods. Usually a simple one, such as Hartree Fock [18] or Car-Parinello Density Functional Theory [28], is chosen and the concerns regarding the QM-region in these simulations are basically the same as what is the case with these methods in other cases. The major difference is that the problem is not solved in gas phase but with a perturbed Hamiltonian to respond to the environment. The terms included in the Hamiltonian are usually an important criterion for the quality of the method. All methods include some electrostatic interaction from the classical region.

$$H = H_o + H_{el.stat.} \quad (3.11)$$

Here H_o is the gas phase Hamiltonian and $H_{el.stat.}$ includes the field from a set of charges in the classical region. Further refinement can also include a polarizable classical region and include the effects of the polarized dipoles in H . The QM-region will react to the position of the surrounding molecules and adapt its electronic structure accordingly. When performing QM/MM methods

on ions in water, the QM-region is usually chosen to be the central ion and at least one shell of water molecules.

The model used in this report, termed QMSTAT will be extensively described later and can be seen as an improvement to current QM/MM models, by also introducing exchange repulsion in the Hamiltonian. That way, it is possible to leave more parts out of the QM-region, since the response of the water molecules is more sophisticated and in some sense more physical than what is the case with QM/MM simulations.

3.8 MOLCAS

MOLCAS [29] is a quantum chemical software package designed to perform high accuracy ab initio calculations. It is developed and maintained by the group for theoretical chemistry at the University of Lund, Sweden. All simulations performed in this report are done using the MOLCAS 6.4. environment where the most important module for this project is QMSTAT, described below, together with a short description of the other modules used.

3.8.1 SEWARD

In every quantum chemical calculations a lot of one and two electron integrals have to be calculated. The amount of two-electron integrals grows with the number of basis functions to the power of four and the calculation, storage and Input/Output-operations related to these may be the bottleneck in large computations [11]. There are two strategies to calculate these integrals. One possibility is to calculate the integral when needed and then delete it afterward. This of course has the disadvantage that when the integral is needed a second or maybe a thousandth time, it has to be recalculated. On the other hand, there are only small memory requirements and Input/Output costs. The other choice is to calculate the integrals before the simulation and store them on disk for later use. When an integral is needed in a calculation, one block containing the desired integral is imported into the main memory. How to sort the integrals, so that this block contains integrals, needed at the same time, is one of the main concerns when deciding how to calculate these integrals. This is because the main problems with this method are large memory requirements and more computer time spent on Input/Output-operations than for the direct calculations. This is nevertheless the conventional way to solve the one and two electron integrals. MOLCAS is focused on the latter strategy and before every QM -calculation the one and two electron integrals are calculated by the module SEWARD. SEWARD also calculates the interaction energy between the cores and estimates the kinetic energy of the electrons. The two electron integrals are calculated using Rys quadrature [30] while the one-electron integrals are calculated using the Gauss-Hermite quadrature [31].

3.8.2 MC-SCF and CI

In a normal SCF calculation, all electrons are located in doubly occupied orbitals. To include electron correlation, one possibility is to include Slater determinants where one or more electrons have been excited in the energy minimization. It is then postulated that the wave function of the system can be written as a linear combination of a set of electronic states.

$$\Psi = \sum_i c_i \Psi_i \quad (3.12)$$

Then there are two principal choices on how to find Ψ . If only the coefficients in equation 3.12 are optimized to find the minimum energy, the method is called Configurational Interaction. If also the orbital coefficients in the Slater determinants from equation 3.7 are optimized simultaneously the method is called Multi Configurational SCF (MC-SCF) [11].

It is usually impossible to include all possible excited states in equation 3.12 and in some sense we have to make a selection of which states to include. One possibility is to include all single and double excitations using CI, this is called CISD, Configurational Interaction with Single and Double excitations. This method can be improved by including Triple and Quadruple excitations to give CISDT and CISDTQ respectively. In this report we have used two other MC-SCF approaches, CASSCF and RASSCF, described below.

3.8.3 Complete Active Space-SCF

In the CASSCF-approach [32], the orbitals are grouped in three groups

- Inactive doubly occupied orbitals, these are treated the same way as in SCF.
- Active orbitals
- Inactive empty orbitals

In addition we have to choose a number of active electrons. The inactive doubly occupied orbitals are treated exactly the same way as in SCF. The same is true for the inactive empty orbitals. In the active orbitals we must include at least enough orbitals to make room for the active electrons. In addition to the SCF ground state we find all possible states that are achievable when permutating the electrons in the active orbitals and we say that our CASSCF ground state is the linear combination of these that give the lowest energy.

3.8.4 RASSCF

RASSCF [33] is an acronym for Restricted Active Space Self Consistent field and is a modification of CASSCF. In CASSCF, all possible excited states within the active space are included. This can easily give an untreatable amount of excited states. In RASSCF the active space is therefore further divided into three parts:

- RAS1: A set of orbitals that are doubly occupied in the SCF ground state and only a threshold number of electrons is allowed to be excited from this space.
- RAS2: A set of orbitals that may or may not be occupied in the ground state and from which and to which, an arbitrary number of electrons can be excited.
- RAS3: A set of orbitals, unoccupied in the ground state, into which, only a threshold number of electrons are allowed to be excited.

This way the number of states can be reduced by many orders of magnitude by neglecting states where many electrons are excited at the same time. States with many excited electrons are likely to be high in energy and would thus not have influenced the result of a CASSCF calculation.

3.8.5 RASSI

RASSI is an acronym for Restricted Active Space State Interaction and is a module of MOLCAS. Given a set of partly overlapping RASSCF states, RASSI can produce an orthogonal basis spanning the same subspace in an efficient manner [34]; the method is also called CASSI when applied to CASSCF states instead of RASSCF. E.g. when the ions are modeled, we use as basis the unperturbed ground state of the free ion, together with the ground state in a small electric field. These states will be highly overlapping, but since it is easier to work with orthogonal states, we use RASSI to give us that.

3.8.6 MPPROP

In the QMSTAT approach, all Coulombic interactions are treated in a multipole expansion. Instead of calculating the exact interaction energy between two charge distributions we multicenter multipole expand the distributions and calculate the interaction energy between these. This procedure is done using the MOLCAS module MPPROP.

3.8.7 FFPT

FFPT is a module for adding a perturbation to the wave function in MOLCAS. In this work it is used to introduce an electric field or a field gradient to give basis orbitals for the calculations. This is done by altering the V_{ext} in equation 3.1.

3.8.8 MP2 and CASPT2

MP2 [35] and CASPT2 [36] are both used to calculate the second order perturbation estimate for the energy of a system. As input these programs use a SCF or CASSCF solution respectively.

3.9 QMSTAT

We run a quantum mechanical Monte Carlo (MC) simulation of cations in the QMSTAT module [6]. QMSTAT is an acronym for Quantum Mechanical /Statistical Mechanical, meaning that a simulation is run treating one part of the system at a quantum mechanical level, while the rest, the solvent, is treated at a statistical mechanical level. In our case we divide the system into three interacting parts:

- The QM-region, which in our case only consists of a single ion
- The discrete solvent region containing 100 NEMO water molecules
- The dielectric continuum representing the bulk water phase

and we run a MC simulation of a system consisting of these three. The only quantity required by the MC algorithm is the energy in every step and thus this is the central quantity to be calculated. There are well established methods for calculating the energy of each of the three regions by itself and also for calculating the interaction energy between the QM-region and dielectricum and between the discrete water region and the dielectricum. The problem lies in how to couple the quantum mechanical ion with the force field described water molecules. We will start with the established parts and return to the coupling problem later.

3.9.1 The QM-region

Firstly, the QM-region will be described for itself. We run a MC simulation for several million steps. In each of these steps we in some sense have to solve the time independent Schrödinger equation to get the energy of the ion. This naturally means that we cannot afford to choose the most complex model to model the central ion. Two different approaches are used depending if we are studying a closed shell SCF system or a MC-SCF system.

SCF QM-region If the QM-region is described at the SCF level, a normal SCF calculation is performed in each MC-step. To generate the basis set for the SCF calculation, we first perform a single calculation in vacuum and others in different potentials, e.g. an electric field or field gradient. The density matrices describing the solutions in these environments are averaged and the averaged density matrix is diagonalized to give a set of orbitals. These are taken as the basis in the QMSTAT simulation.

RASSCF QM-region If the QM-region is described at the RASSCF level, a different approach is adapted. Instead of taking single electron spin orbitals as basis functions, we use electronic wave functions for the entire system in different excitation levels and different environments, mimicking the disturbances from the environment we expect will surround the QM-system. That is, before we start the simulation, we solve the Schrödinger Equation for the electron structure in the ground state and a number of excited states. Then we solve it in an environment, e.g. an electric field, field gradient or a well potential. The latter examples will give a polarized wavefunction, a wavefunction with an induced quadrupole and a spatially contracted wavefunction respectively. Our basis consists of all these molecular wavefunctions Ψ_i . We now make a linear Ansatz that the wave function can be written as a linear combination in our basis

$$\Psi_i^{QM} = \sum_j c_{ij} \Psi_j \quad (3.13)$$

The electronic structure in a random environment now has the ability to be polarized, induce a quadrupole or contract depending on the environment in order to minimize the system energy. Of course the choice of basis functions will have consequences for the resulting properties. It is necessary to include as many basis functions as possible to include all relevant effects, while still keeping the number of basis functions as low as possible to minimize the computational costs.

3.9.2 NEMO Water

Before we describe how the surrounding influences the QM-region, we describe the surrounding, in our case water, by itself. The interaction energy of the NEMO water can be partitioned into four parts

$$E = E_{ele} + E_{ind} + E_{rep} + E_{disp} \quad (3.14)$$

The first term is the electrostatic interaction. This is modeled as four charges, two positive on the hydrogens and two negative close to oxygen, placed to reproduce the dipole moment and quadrupole moment of SCF water in gas phase. The next term represent the energy of induced dipoles. Linear isotropic polarizabilities are placed on the three atomic centers and the energy of the

induced dipoles is calculated iteratively for all the water molecules. The third term is an exchange repulsion term with one exponentially decaying part and one polynomial part and the exchange repulsion between two molecules A and B is written

$$E_{rep}^{AB} = \sum_{i \in A} \sum_{j \in B} a_{ij} e^{-b_{ij} r_{ij}} + \left(\frac{c_{ij}}{r_{ij}} \right)^{20}, \quad (3.15)$$

where r_{ij} is the distance between the two atoms i and j . a , b and c are parameters. The last term is the attractive dispersion energy written as

$$E_{disp}^{AB} = - \sum_{i \in A} \sum_{j \in B} \left(\frac{d_{ij}}{r_{ij}} \right)^6 S(r_{ij}), \quad (3.16)$$

where

$$S(r) = 1 - e^{-(r/e)^n} \quad (3.17)$$

is introduced to damp the dispersion on short distances. For more information regarding the different terms and values of the parameters see [37].

3.9.3 The interaction with the dielectric medium

Our droplet, consisting of an ion and 100 water molecules, is placed in a dielectric medium, a medium that does not conduct electricity but will be polarized in response to charges nearby. This is a simplified picture of the bulk water phase in the simulations. Some water molecules are introduced explicitly, but the action from the rest is averaged out and acts on the QM-region and the other water molecules as a continuum. A positive charge near the edge of the dielectric will polarize the medium in such a way that negative charge allocates in the vicinity inside the dielectric medium. This negative charge will produce an electrostatic potential, also called reaction field in the cavity. To solve these interactions numerically exact would be computationally very expensive. Instead the interactions are calculated with the image charge approximation [38]. This approximation utilizes the fact that the response from the dielectric medium to a charge nearby can accurately be approximated by a charge of opposite sign in the medium. This image charge creates a reaction field in the cavity which interacts with the charges there. The water molecules and the QM-region have an identical interaction with the dielectric through their charge distributions.

A charge, whether positive or negative will be attracted to the dielectric because of the image charges located there. This attraction should be balanced by the attraction between explicit water molecules, but still, if nothing is done to prevent it, water molecules will approach the discontinuity. To avoid water molecules leaving the cavity, an additional potential barrier, exponentially increasing with the distance to the edge is added near the boundary. The reason

for choosing this form is not physical, but motivated from the fact that the distance to the edge is already calculated when calculating the effect of the image charges.

3.9.4 How the water molecules influence the QM-region

The QMSTAT model includes most of the water influence as a perturbation to the Hamilton operator written as

$$H = H_o + H_{ele} + H_{ind} + H_{rep,S^2} \quad (3.18)$$

The first term is here the unperturbed gas phase Hamiltonian as it would be for the free QM-region as given in equation 3.2.

The second is the disturbance due to the four charges on each water molecule described in section 3.9.2. The term is purely Coulombic and is written as

$$H_{ele} = \sum_{i,s} \frac{q_i^s}{|\mathbf{r} - \mathbf{r}_i|}, \quad (3.19)$$

where the summation is over the four charges q_i on all the water molecules s .

The third term is the interaction energy with the induced dipoles of the water molecules and is written as

$$H_{ind} = \sum_{j,s} \frac{\boldsymbol{\mu}_j^s \cdot \hat{\mathbf{r}}}{|\mathbf{r} - \mathbf{r}_j|^2}, \quad (3.20)$$

where $\boldsymbol{\mu}_j^s$ is the induced dipole of the atomic center j on water molecule s . $\hat{\mathbf{r}}$ is the unit vector from the point dipole. The way the dipoles influence the QM-region is similar in fashion to the permanent charges, but this term makes it necessary to solve the Schrödinger equation and the induced dipoles in an iterative fashion. First a guess is made for the induced dipoles and the Schrödinger equation is solved. This leads to a new set of induced dipoles and the Schrödinger equation is solved in this field. The procedure is repeated until the equations have converged. This method is termed Self Consistent Reaction Field.

The last term is included to take care of the exchange repulsion between the electrons of water and the ones in the QM-region. When there is not substantial overlap between water and the QM-region, the repulsive energy should be proportional to the square of the overlap [39]. This is calculated with a Hamiltonian on the form

$$\langle \Psi_i | H_{rep,S^2} | \Psi_j \rangle = d \sum_{k,s} \langle \Psi_i | \chi_k^s \rangle \langle \chi_k^s | \Psi_j \rangle \epsilon_k \quad (3.21)$$

where χ_k^s is the occupied orbital number k on water molecule s inside a cutoff distance, in these simulations set to 5.3 Å. ϵ_k is the energy of orbital k . To use the energy as a scaling factor is not purely physical but motivated from the fact that an overlap with a strongly binding orbital will be less favorable than the overlap with a more diffuse orbital higher in energy. The negative d parameter in equation 3.21 has to be fitted to reproduce energy curves from supermolecular calculations. The orbitals of water are calculated in a gas phase SCF calculation before the simulation and kept constant in every MC-step.

The charge density and its multipole expansion for all the QMSTAT basis functions has been calculated before the simulation is started. When a solution is found for Ψ , the multipole expansion of the charge density in the QM-region is also known. This expansion will influence the water molecules by polarizing them. This polarization occurs only on the isotropic polarization centers and the orbitals on water will not be influenced by the electronic structure in the QM-region.

In addition to these terms two energy terms are added without being part of the Hamiltonian, that is

$$E_{QM} = \frac{\langle \Psi | H | \Psi \rangle}{\langle \Psi | \Psi \rangle} + E_{disp} + E_{rep,S^6} \quad (3.22)$$

For non-polar systems, the most important attractive term is dispersion or London forces. It can be shown that for closed shell systems on long distances this is an attractive force which decays as r^{-6} [11]. This term is not included at the CASSCF level and is incorporated in the QMSTAT model as an extra energy term. For a charged specie such as Cu^{2+} the contribution of this term is neglectable, but still included in the simulations.

The last term is another exchange overlap term. It can be shown [39] that the exchange repulsion is proportional to the series given by

$$E_{rep} \propto \frac{S^2}{1 - S^2} = S^2 + S^4 + S^6 + \dots \quad (3.23)$$

The first term in this expansion is included in H_{rep,S^2} , and experience from earlier works with ions in water [40] showed that the S^4 term was superfluous. Because of this, a term proportional to S^6 is added. This is implemented as $(S^2)^3$ and a parameter is used to fit the repulsive part of the energy surface. Without this term, the potential curve is not repulsive enough on short distances and the first peak of the radial distribution function will be located at too short distances.

This solution has worked well for previous problems (singly charged ions [40], formaldehyde [41] and acetone), but did not work well for the copper ion. It gave a minimum in the energy surface for Cu^{2+} and 6 water with a too large Cu-O distance. As a temporary solution we swapped this repulsive term with a Lennard-Jones like r^{-12} term. Also here a parameter has to be fitted to supermolecular curves.

There are some approximations that should be emphasized in these procedures. First of all, when a water molecule approaches an ion, both the wave function on water and the one on the ion will change to adapt to the new environment. In our description only the electronic structure in the QM-region relaxes whereas the water molecules remain mostly unchanged. They respond by the polarizabilities on the atomic centers, but the orbitals used to calculate the overlap remains unchanged. Also, none of the electrons relax to minimize the energy to the dispersion and the r^{-12} term, these terms only influence the sampling in the MC-algorithm but does not change the electronic structure.

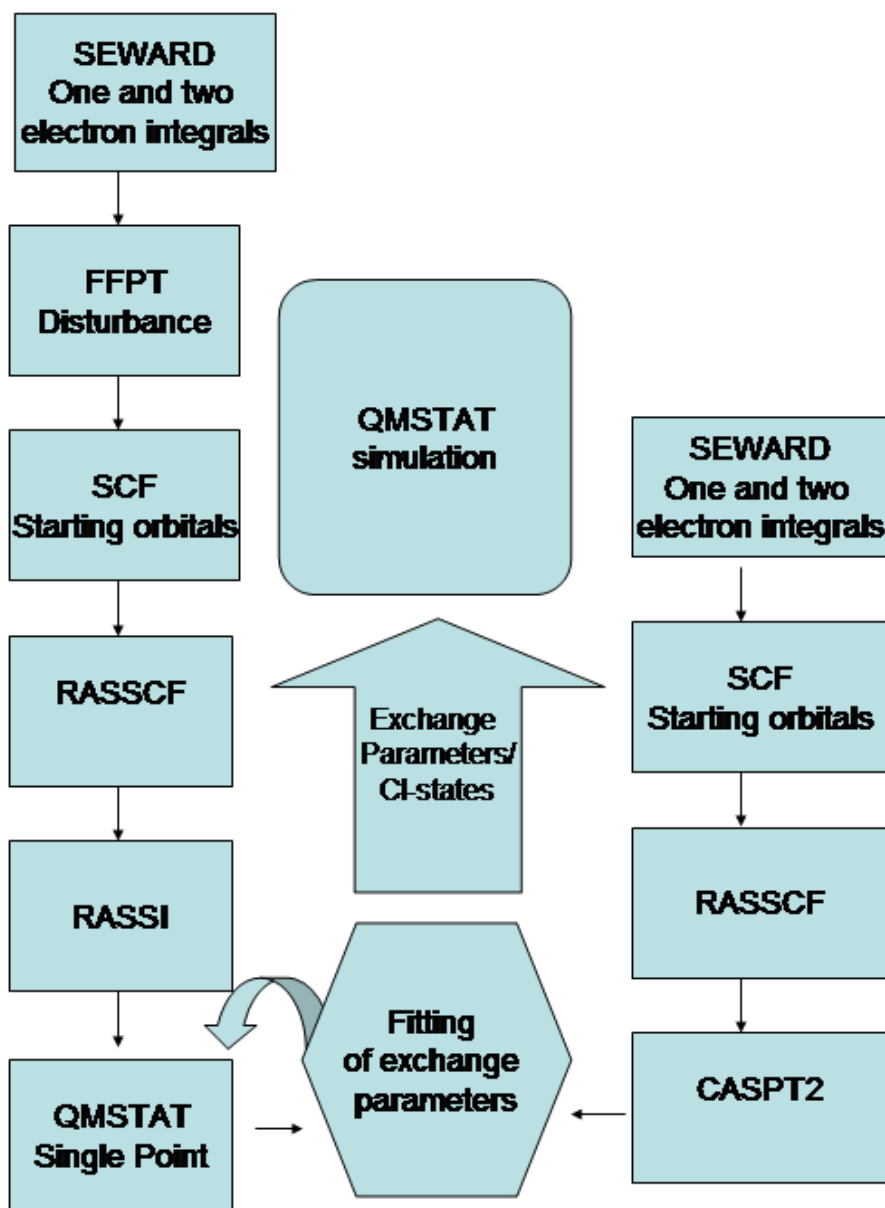


Figure 3.1: Flow chart for calculations when the QM-region is described on the RASCF-level. On the left hand side basis functions for the QMSTAT-simulation are calculated. On the right hand side supermolecular potentials are calculated. The exchange repulsion parameters are fitted so that the QMSTAT-potential reproduces the supermolecular potential before the simulations are performed.

3.10 Float chart for the calculations

In figure 3.1 a float chart of the calculations performed in this report is shown. It contains three major parts. On the left side is the preparation for QMSTAT, the calculations of a set of basis functions, their orthogonalization and calculation of their multipole expansion. In the QMSTAT model parameters are required in the calculation of exchange repulsion. These parameters are fitted to energy curves from supermolecular calculations which are calculated on the right side. These data are combined and a simulation is run using QMSTAT in the middle.

Chapter 4

Previous results

4.1 The hydration of Mg^{2+}

Magnesium complexes are usually hexacoordinated and the ion tends to bind directly to water, also when other anionic ligands are available [42]. It has been seen in DFT studies that when gradually increasing the number of water molecules in supermolecular calculations that the most stable Mg^{2+} -water complex is clearly the octahedral hexacoordinated one with the water molecules located between 2.10 and 2.12 Å [42, 43].

Experimental studies with NMR [44], X-Ray Diffraction [45] and Raman spectroscopy [46] also give the same CN.

One QM/MM simulation of the ion with 199 water molecules has given a CN of 6 and $r_{\text{Mg}-\text{O}} = 2.03$ Å [47].

4.2 The hydration of Ca^{2+}

The hydration of Ca^{2+} is of great interest because of its biological activity as a neural transmitter, building block of bones and importance in blood clotting. Both theoretical and experimental studies have been performed to determine the coordination of water molecules around the ion. Nevertheless, in contrast to Mg^{2+} , there is still dispute over the coordination number and the distance to the closest water molecules. One of the main reasons for this is that the coordination structure of Ca^{2+} is much more dynamic than what is the case for Mg^{2+} , and no definite, only an average CN can be given.

X-Ray diffraction experiments have found a CN between 6-8 and $r_{\text{Ca}-\text{O}} = 2.39 - 2.43$ Å [48].

Neutron diffraction experiments have been performed and the data has been interpreted to give a CN between 6.4 and 10 with $r_{\text{Ca}-\text{O}} = 2.39 - 2.46$. The

CN was found to increase with decreasing concentration of Ca^{2+} [49].

A combined study using EXAFS, Long Range XD and MD concluded with a CN of 8 and $r_{\text{Ca-O}} = 2.46 \text{ \AA}$ [50].

One Car-Parinello Molecular Dynamics simulation ran for a time period of 7 ps and found a constant CN of 6, with the RDF going to zero between the first and the second coordination shell. The reason for this may very well be that the simulation is trapped in a local energy minimum. The location of the first maximum in the RDF is at 2.45 \AA in agreement with experimental data [51].

Another QM/MM simulation ran for 14 ps starting from a six-coordinated structure obtained CN = 7-8 and with four occurrences of water molecules either entering or leaving the first coordination shell. From this it is estimated that the mean residence time of a water molecule in the first coordination shell is of the order of magnitude 10 ps. $r_{\text{Ca-O}}$ is found to be 2.6 \AA , significantly larger than the experimental values and other MD simulations [52].

Classical MD simulations have been performed giving CN between 8 and 9.3 and $r_{\text{Ca-O}}$ between 2.39 and 2.53 \AA [51].

The reason for the dispute of the coordination number may be that there is dynamical equilibrium between more states with different CN. This makes it difficult to find the coordination structure using computationally intensive methods like QM/MM because it is difficult to run a long enough simulation spanning over a large amount of changes in coordination structure.

4.3 The hydration of Sr^{2+}

There are less experiments performed on Sr^{2+} than on any of the other ions studied. X-ray experiments of SrCl_2 solutions show an average CN of 7.9 and a $r_{\text{Sr-O}} = 2.60 \text{ \AA}$ [53, 54]. EXAFS data has shown 8 water molecules in the first coordination shell and $r_{\text{Sr-O}} = 2.57 \text{ \AA}$ [55].

4.4 The hydration of Cu^{2+}

The hydration of the hydrated Cu^{2+} ion has also been extensively studied. It is usually seen as a classical example of the Jahn-Teller effect and is believed to be hexacoordinated in water with four short and two longer Cu-O distances.

A SDCI study of the cluster of copper and six water find a minimum energy structure with four oxygens at a distance 1.94 \AA from Cu and two oxygens at a distance of 2.43 \AA which also is in good agreement of the classical picture of the ion in water [56].

More authors have discussed the solvation structure of copper using neutron diffraction. The neutron diffraction data shows some water molecules at a distance between 1.94 - 2.00 \AA from the positive ion. Then there is more dispute

as to where the next water molecules are located. Different authors state that the second closest waters are located from 2.12 Å to 2.60 Å. The coordination is usually assumed to be an elongated octahedron with CN = 6 [8, 57]. The dispute in structure indicate a dynamic system which might be quickly alternating between different structures, e.g. which water molecules that at a given time are closest to the ion.

A combined theoretical and experimental study using Neutron Diffraction, Car-Parinello simulations with the BLYP functional [58, 59] and reinterpretation of old experimental data concluded with a coordination number of five [60]. This study has, however been criticized for the simplicity of the BLYP functional [61].

Even though most Cu^{2+} complexes are known to be hexacoordinated, a sandwich di-crown ether Cu^{2+} complex has been synthesized where the central ion is pentacoordinated [62].

Since copper has a d^9 -electronic structure with splitting between two sets of d -orbitals it also has the ability to absorb electromagnetic radiation in the visible/near-IR range and is the reason why solutions of copper have a blue color. This IR-spectrum is given in figure 4.1.

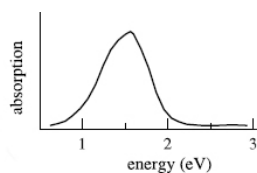


Figure 4.1: The experimental IR absorption spectrum for Cu^{2+} in water [63].

Chapter 5

Computational details

5.1 Supermolecular calculations

5.1.1 Ca^{2+} with one water molecule

A supermolecular calculation was performed using the NEMO water geometry, with the water molecule pointing with the oxygen atom toward Ca^{2+} . The oxygen-calcium distance was varied between 1.5 and 6 Å. To correct for basis set superposition error, the results were counterpoise corrected [64]. At each geometry, starting orbitals were found using an SCF calculation, then the energy was optimized using MP2. The ANO-s basis set was used [65]. For Ca^{2+} we used $17s12p4d$ contracted to $7s7p4d$, for oxygen $10s6p3d$ contracted to $7s6p3d$ and for hydrogen $7s3p$ contracted to $4s3p$.

5.1.2 Mg^{2+} with one water molecule

The same procedure and basis set for water was used with magnesium as described in section 5.1.1. For the magnesium ion the ANO-s basis set was used, $13s8p3d$ contracted to $7s6p3d$.

5.1.3 Sr^{2+} with one water molecule

With strontium we used the ANO-rcc [66] basis set for both the ion and the water molecule, because the ANO-s basis set does not include optimized orbital coefficients for elements heavier than Kr. For Sr we used $23s19p12d4f$ contracted to $11s10p7d4f$, for oxygen $14s9p4d3f2g$ contracted to $7s6p3d1f$ and for hydrogen $8s4p3d1f$ contracted to $4s3p1d$. The same geometries were used as in section 5.1.1. Calculations done with this basis set are relativistically corrected with the method of Douglas and Kroll [67].

5.1.4 Cu^{2+} with one water molecule

For Cu^{2+} the supermolecular calculations were performed in the same geometries as in section 5.1.1, but since Cu^{2+} has a d^9 open shell electronic configuration neither closed shell SCF nor MP2 can be used. Instead we used a CASSCF calculation with the five $3d$ orbitals in the active space and the rest of the orbitals inactive. After this, a CASPT2 calculation was performed to include the effect of electron correlation. The ANO-s basis set was used for all atoms. For Cu^{2+} we used $17s12p9d4f$ contracted to $7s6p5d3f$, for oxygen $10s6p3d$ contracted to $7s6p3d$ and for hydrogen $7s3p$ contracted to $4s3p$.

5.1.5 Cu^{2+} with six water molecules

Supermolecular calculations were for Cu^{2+} also performed using six water molecules to see whether many-body terms were incorporated correctly in the QMSTAT potential. The same basis set and method as in section 5.1.4 were used. The geometries sampled are shown in figure 5.1 where we vary the axial distance to two of the water molecules and the equatorial distance to the other four. The calculations were performed in D_{2h} symmetry, the maximum symmetry allowed in MOLCAS.

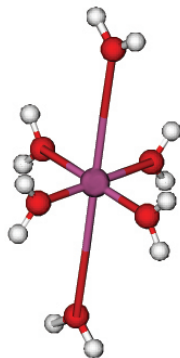


Figure 5.1: The geometries sampled in the supermolecular calculations with Cu^{2+} and 6 water molecules were obtained by varying the axial distance to two of the water molecules and the equatorial distance to the other four.

5.2 Simulations

5.2.1 Mg^{2+} in water

For all the earth alkali metals we used the SCF treatment of the QM-region. For magnesium, our QMSTAT molecular basis functions were chosen to be the SCF ground state in vacuum and the six ground states found when the ion was placed in an electric field of ± 0.002 a.u. ($0.103\text{V}/\text{\AA}$) along each of the coordinate axes.

The basis set used in the calculations were the same as in the supermolecular calculations described in section 5.1.2. The simulations were started from three different configuration found for Cu^{2+} surrounded by six water molecules in the first coordination shell. The structures were allowed to equilibrate for 100,000 Monte Carlo steps before three parallel simulations of 900,000 million steps each, were performed.

5.2.2 Ca^{2+} in water

The procedure described in section 5.2.1 was also applied in the simulations of Ca^{2+} . The starting structures were taken from three different simulations with Cu^{2+} , both penta- and hexacoordinated.

5.2.3 Sr^{2+} in water

The procedure described in section 5.2.1 was also applied for Sr^{2+} , but this time with starting structures from simulations run with Ca^{2+} , with a 7-coordination.

5.2.4 Cu^{2+} in water

For Cu^{2+} the MC-SCF description of the QM-region was used and three different procedures to create a Molecular Basis were attempted.

The 5-state basis functions

As mentioned, the Cu^{2+} ion has a d^9 electronic structure. For the free ion there are five ways to accomplish this; The $3d$ -electrons can be perturbed so that the hole is positioned in any of the five degenerate d -orbitals. Our simplest choice of basis consists of only these five states. To create them a CASSCF calculation was performed with the active space consisting of the five d -orbitals and nine d -electrons, optimizing the orbital coefficients to minimize the sum of the energy of the five lowest states. These five degenerate states were taken as our basis that we termed *5-state*. This basis is not polarizable, since all the d -states have a net dipole moment of zero, nor can it contract or expand, since the radial extension of all the d -orbitals are equal. The only flexibility is where to place the hole in the d -orbitals.

The polarizable basis functions

As for the earth alkali ions, it was wanted to incorporate some degree of polarizability of the ion. To do this, we created a basis consisting of 35 molecular basis functions in the following way; Firstly we included the five basis functions from the 5-state basis set. Secondly, an electric field of ± 0.002 a.u. ($\pm 0.103\text{V}/\text{\AA}$)

along each of the coordinate axes was applied and a CASSCF calculation was performed in each of these environments. The basis set and procedure being the same as in vacuum. In each of the environments five basis functions were obtained giving a total of 35. This was taken as the *polarizable* basis functions.

The single state basis functions

To allow for some flexibility in the spatial extension of the ion orbitals, we created a set of orbitals located in a potential well. The well consisted of a sum of spherical Gaussian functions and had the form shown in figure 5.2. The basis functions up until now were found by minimizing the average energy of the five lowest states. A different approach is to alter the basis function coefficients to minimize the energy of each state independently. This was done by first performing an average calculation and then follow each of the roots separately to the nearest energy minimum. Such local minimum calculations always have a risk for falling down into the wrong minimum, but the calculations converged to the correct minima in this case. By this procedure we created a basis with ten basis functions. The five lowest states with the potential well present and the five lowest without it.

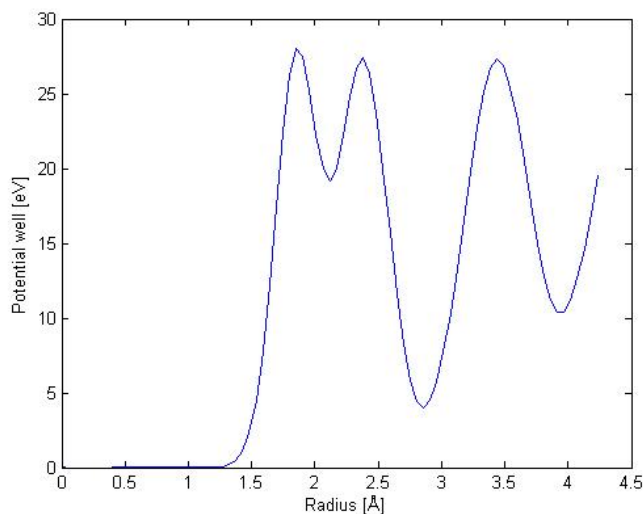


Figure 5.2: The spherical potential used to limit the diffuse electronic density of Cu^{2+} . Note that even though the potential drops around 2.7 Å it is never below 4 eV and the electronic density is also here zero.

5.3 Data Analysis

5.3.1 The Radial Distribution Function

The number density of a specie A in a solution, is given by $\rho_A = N_A/V$, where N_A is the number of particles of type A and V is the volume. This is also called the singlet distribution function noted by n_A . A pair distribution function $n_{AB}(r)$ is defined as the probability density of finding a particle of type A at a given point and a particle of type B at another point separated from the first by r . The radial distribution function (RDF) is defined as

$$g_{AB}(r) = \frac{n_{AB}(r)}{n_A n_B}. \quad (5.1)$$

When the distance r grows large, the probability of finding the two particles in the two volume elements becomes the product of finding the two particles there irrespective of each other and the RDF approaches one.

5.3.2 Estimating absorption spectra

In the RASSCF treatment of the QM-region a RASSI matrix is calculated in each MC-step. The eigenstate of this matrix with the lowest energy is our ground state and its eigenvalue is the ground state energy of the QM-region. The next eigenstates are excited states in our RASSI-basis in exactly the same environment as the ground state, whereof the first five corresponds to different permutations of the nine electrons in the d -orbitals. These states are orthogonal to the ground state and are estimates to the real excited states. A physical excitation would have given a wavefunction for the entire system orthogonal to the ground state, but since we only have electronic flexibility in the QM-region the best approximation is a state which is orthogonal here.

An excitation is called vertical when the positions of the nuclei are constant and the electronic degrees of freedom are allowed to relax. In QMSTAT this could have been mimicked by solving the Schrödinger equation and the polarization equations for water in an excited state. This was attempted for all the sampled configurations in the simulations with Cu^{2+} , but failed because of divergence in the polarization equations for water for some configurations. A second attempt was made by just calculating the first five eigenvalues of the RASSI matrix. It was seen that in the cases that did converge, the difference between this method and the one where the dipoles of water was allowed to relax was neglectable.

In each of the sampled configurations, we calculate the energy difference between the ground state and the first four excited states. Then a histogram is made with the density of energy gaps and this is called density of states and is taken an estimate to the absorption spectrum.

It should be noted here that the transition dipole moment for a $d \rightarrow d$ transition is exactly zero for pure d -states and therefore no transition will occur [11].

Nevertheless, when we place the system in the asymmetric environment like the explicit water molecules, the external field could give rise to a non-zero transition dipole moment. These have not been calculated in this report but would be needed for a better estimate of the spectrum.

Chapter 6

Results

6.1 Supermolecular calculations

6.1.1 Mg^{2+} and one water molecule

The MP2 and SCF potentials calculated for Mg^{2+} and a water molecule are shown in figure 6.1. It can be seen from the figure that the potential becomes less attractive when electron correlation is introduced with MP2. The reason why this happens is believed to be stemming from the fact that the dipole moment for water is larger in a SCF description than in MP2, which gives a more attractive potential.

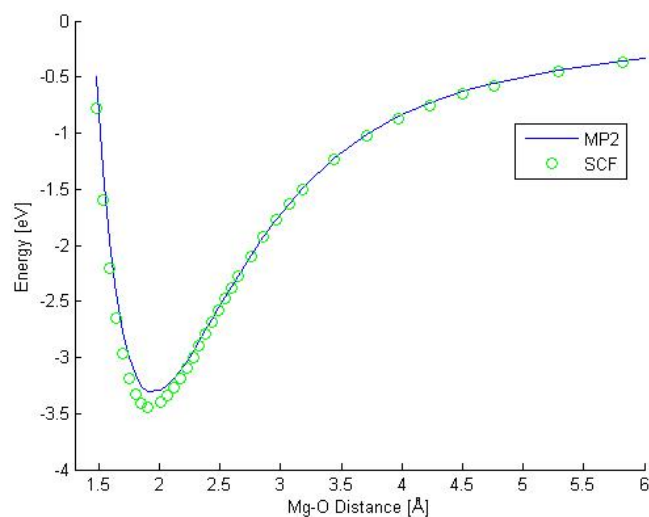


Figure 6.1: The MP2 and SCF potential of Mg^{2+} - OH_2 .

6.1.2 Ca^{2+} and one water molecule

The MP2 and SCF potentials calculated for Ca^{2+} and a water molecule are shown in figure 6.2. The same effect is seen here as for Mg^{2+} , the association energy is higher when introducing electron correlation using MP2. We also see that the potential minimum is not as close nor as deep as for Mg^{2+} . Both these effects are expected because of the larger size of Ca^{2+} , which is a consequence of the $3s$ and $3p$ electrons present in Ca^{2+} but not in Mg^{2+} . It is also seen that on distances further away than 3 \AA , the potentials are almost identical for the two ions, this because the dominating part in the potential is that between a positive charge of 2 and the dipole of water.

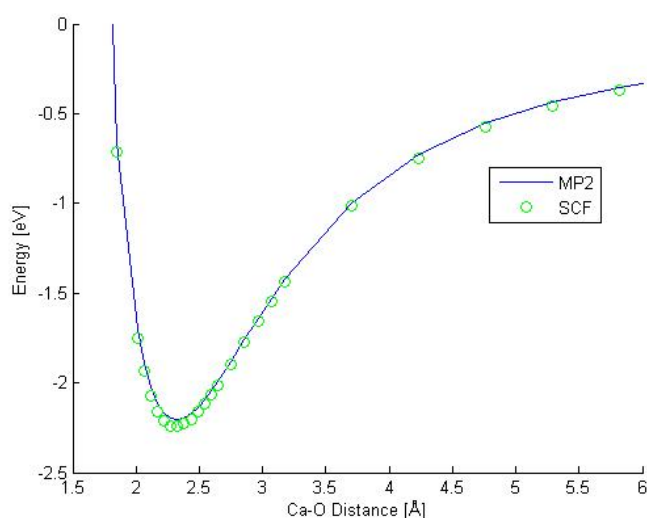


Figure 6.2: The MP2 and SCF potential of $\text{Ca}^{2+}\text{-OH}_2$.

6.1.3 Sr^{2+} and one water molecule

The MP2 and SCF potentials calculated for Sr^{2+} and a water molecule are shown in figure 6.3. We see now that the MP2 association energy is larger than the SCF, but still it lies above at long distances. The effect of a larger dipole moment in the SCF-treatment is still seen on long distances, but this effect is countered by the stabilizing electron correlation effect from MP2 at short distances when the charge distributions are highly overlapping. We also see that the trend started when going from Mg^{2+} to Ca^{2+} is continued when moving another row down in the periodic system. The

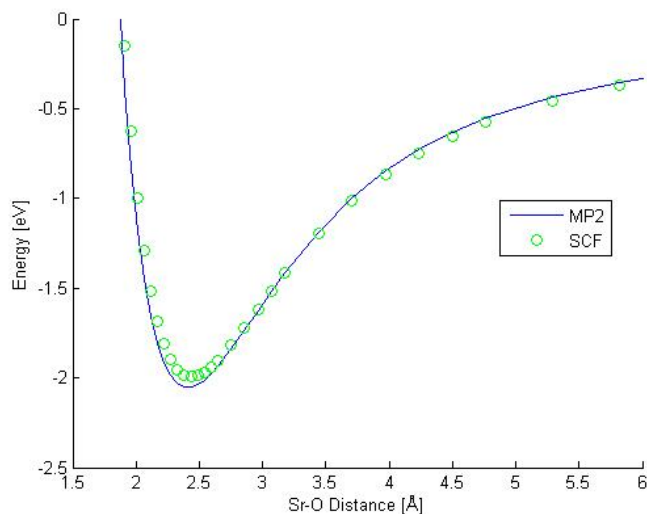


Figure 6.3: The MP2 and SCF potential of $\text{Sr}^{2+}\text{-OH}_2$.

6.1.4 Cu^{2+} and one water molecule

The CASSCF and CASPT2 potentials of Cu^{2+} and water are shown in figure 6.4. It is seen here that the interaction energy between Cu^{2+} is almost the double of what is seen for Calcium. This is due to the higher charge of the copper core and the fact that all the electrons are still in the third shell. This gives a smaller radius and thus a larger electrostatic interaction. In addition to this, Cu^{2+} has the hole in the $3d$ -shell. This will be located along the Cu-O axis, hereby the exchange repulsion and allows for the water molecule to approach closer to the ion. We also see by the difference in the potential between CASPT2 and CASSCF that a significant part of the potential is due to electron correlation, a term that is not included in the QMSTAT model.

6.1.5 Cu^{2+} and six water molecules

The results from the CASPT2-calculation is shown in figure 6.5. The Jahn-Teller distortion of the supermolecule is seen by the energy surface. No minimum is found with six equal Cu-O distances; instead the complex can relax by either elongating or compressing the axial waters. It is also seen that the minimum with four close oxygens is lower in energy, and apparently includes a broader range of states than what is found for two close oxygens. This should indicate that if Cu^{2+} is hexacoordinated it would adopt a 4+2 confirmation. The energy difference however, is only 0.1 eV or approximately 4 kT, meaning that entropic effects can have an important effect on the equilibrium structure. Because distant water molecules have more rotational freedom than water molecules trapped closer to Cu^{2+} one would expect that the 2+4 structure would be

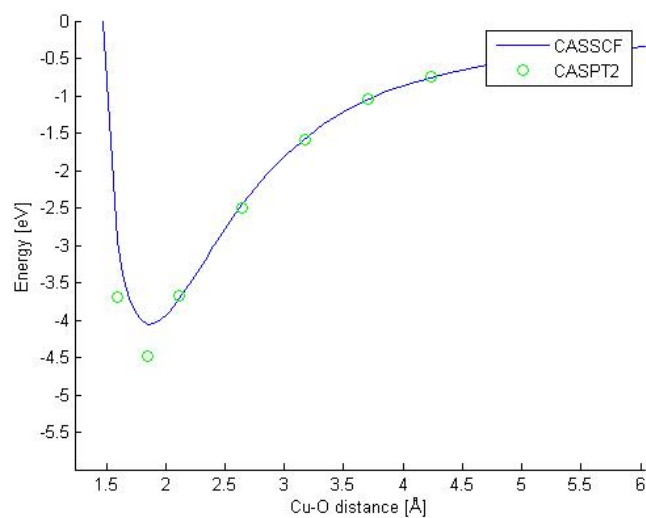


Figure 6.4: The CASSCF and CASPT2 potential of $\text{Cu}^{2+}\text{-OH}_2$.

entropically favored compared to the 4+2 structure. This effect can be on the order of magnitude of the energy difference between the two structures.

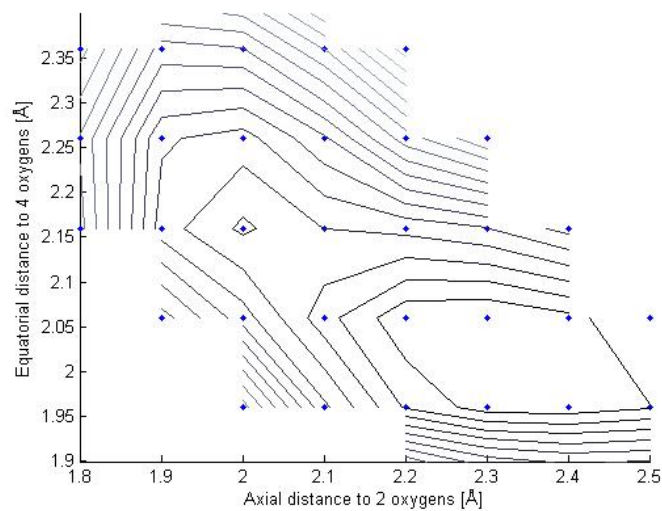


Figure 6.5: Energy surface for $[\text{Cu}(\text{H}_2\text{O})_6]^{2+}$, calculated on the CASPT2 level with D_{2h} -symmetry. Every contour line represents an energy difference of 0.05 eV ($k_bT = 0.026$ eV). The energy has been evaluated in the blue points and linearly interpolated between these.

6.2 QMSTAT potentials

6.2.1 Mg^{2+} and one water molecule

In figure 6.6 the potential used in the QMSTAT simulations is shown together with the MP2 potential. It can be seen that the QMSTAT potential without exchange repulsion added, goes toward minus infinity at short distances. When the H_{S^2} -exchange repulsion term with an optimized d coefficient is added to the Hamiltonian, the potential is well described from the energy minimum and out, but closer than this it is not repulsive enough. This is expected since the assumption that the exchange repulsion is proportional to the overlap squared, only holds when the overlap is small. With the last repulsive, scalar term added, the MP2 potential curve is nicely described. The QMSTAT potential, however, is slightly higher in energy than the MP2 potential at distances between 2 and 3 Å. This is an effect seen even without the exchange repulsion terms added, meaning that it can not be improved by altering these parameters. Nevertheless, the difference is small, but it indicates a problem with the electrostatic description in QMSTAT. Since we in QMSTAT use only an SCF description of the water molecules we have not included electron correlation and thus the potential will more strongly resemble that of the SCF-calculations.

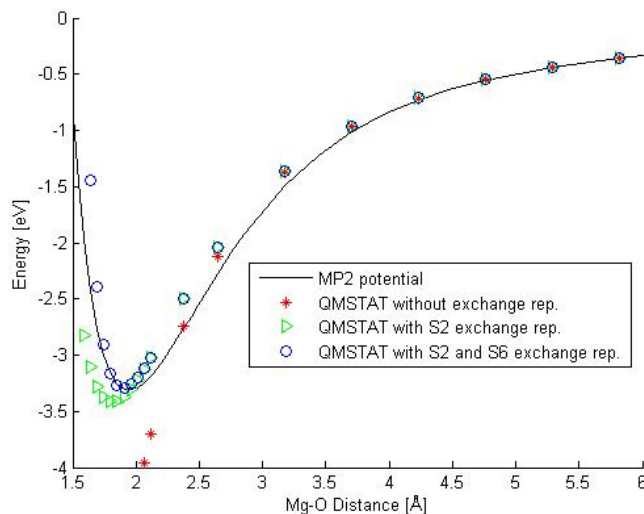


Figure 6.6: The QMSTAT energy surface of Mg^{2+} and a water molecule.

6.2.2 Ca^{2+} and one water molecule

In figure 6.7 the potential used in the QMSTAT simulations is shown together with the MP2 potential. Also here the QMSTAT potential is slightly higher than the MP2 potential, but less so than for Mg^{2+} . It is also seen that the

QMSTAT curve for Ca^{2+} gives a better fit to the MP2 potential.

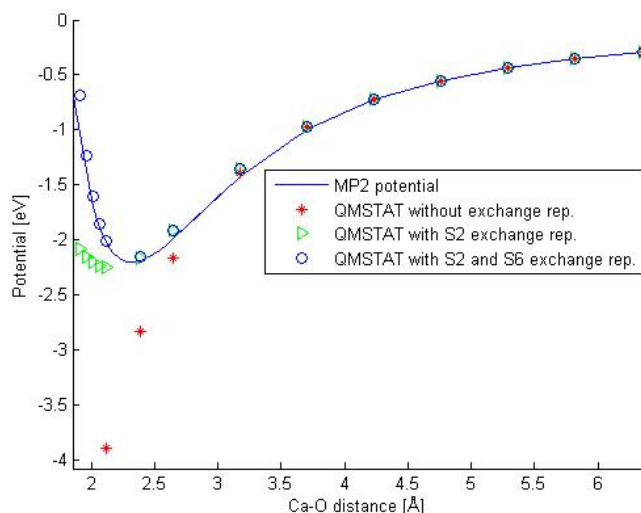


Figure 6.7: The QMSTAT energy surface of Ca^{2+} and a water molecule.

6.2.3 Sr^{2+} and one water molecule

In figure 6.8 the potential used in the QMSTAT simulations is shown together with the MP2 potential. Here we see that we have an almost perfect fit with the calculated potential. The reason for this could be related to the fact that the SCF and MP2 curves for Sr are more similar than what is seen for the other ions, meaning that our treatment without electron correlation is better in this case.

6.2.4 Cu^{2+} and one water molecule

The 5-state basis functions The QMSTAT potential for a water molecule and Cu^{2+} is shown in figure 6.9. What is seen here is that even without the added exchange repulsion the QMSTAT potential is too high at distances outside the minimum. The effect here is larger than for Mg and it is likely that it is necessary to include more than the 5 RASSI states here included to get a sufficient description of the ion.

Polarizable basis functions

When the polarizability is added more of the potential curve is described as shown in figure 6.10, but the QMSTAT-potential is still above the CASPT2-potential, but less than what is the case with the 5-state basis functions.

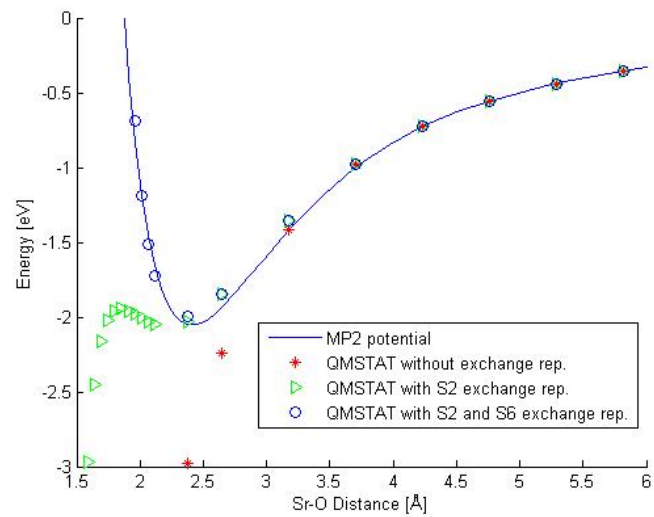


Figure 6.8: The QMSTAT energy surface of Sr²⁺ and a water molecule.

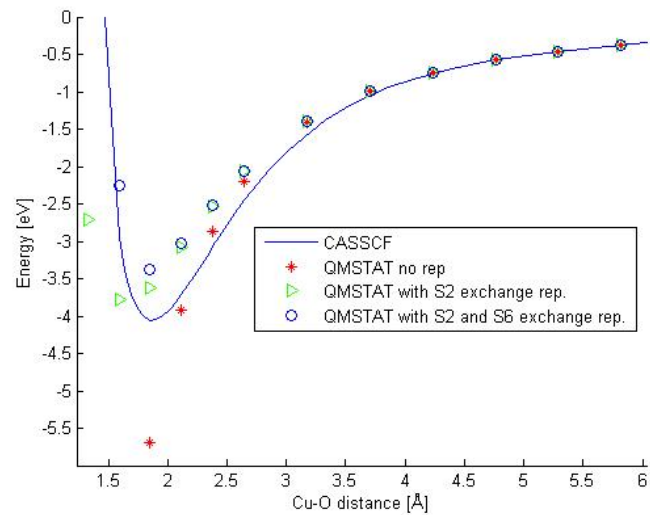


Figure 6.9: The QMSTAT energy surface of Cu²⁺ and a water molecule using the 5 states basis functions

Single state basis functions

This potential is the one that gives the best fit to the supermolecular CASPT2 curve. Still it is seen that we have an overestimation of the energy down to the minimum. It is believed that this overestimation stems from what is termed charge transfer. In the CASPT2 calculations we see that some of the orbitals on water mix significantly with the ones on the ion. There is also some transfer of negative charge from the water molecules to Cu. From a chemical point of view this is the onset of a covalent bond between the species and is not possible to model with the current QMSTAT potential.

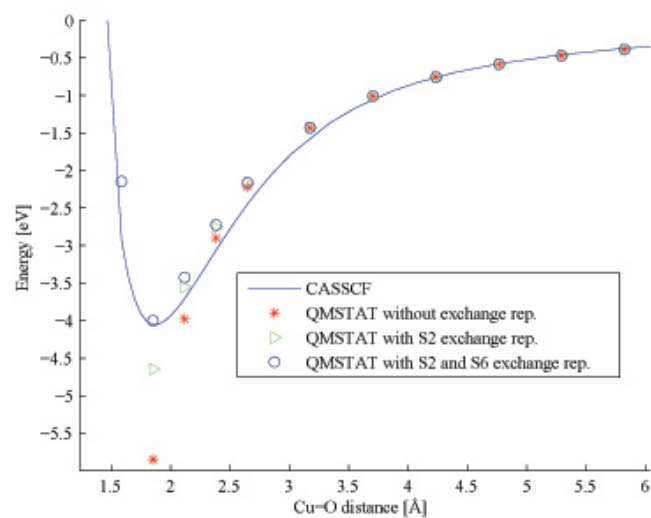


Figure 6.10: The QMSTAT energy surface of Cu^{2+} and a water molecule using the polarizable basis functions

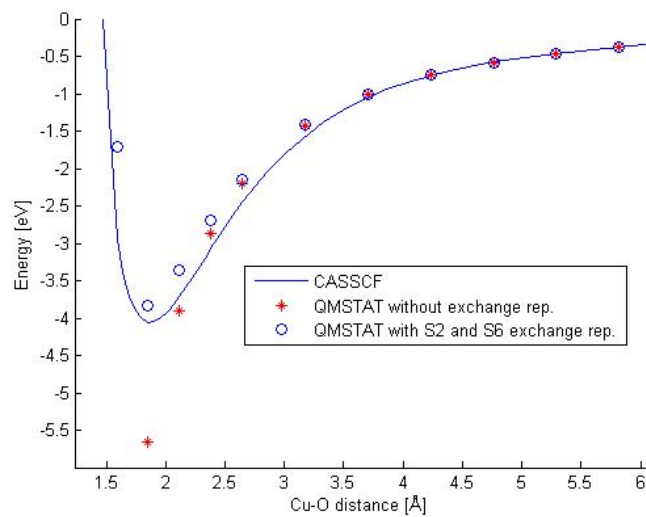


Figure 6.11: The QMSTAT energy surface of Cu^{2+} and a water molecule using the single state basis functions.

6.2.5 Cu^{2+} and six water molecules

The 5-state basis functions

In figure 6.12 the QMSTAT potential obtained for the same configuration as in figure 6.5. We see that the potential for the 2+4 configuration gives a reasonable location of the distance to two innermost oxygens, whereas the location of the next four is too far away from the ion compared to the CASPT2 potential in figure 6.5. In the 4+2 configuration all the water molecules are located too far away from the ion compared to the CASPT2 potential.

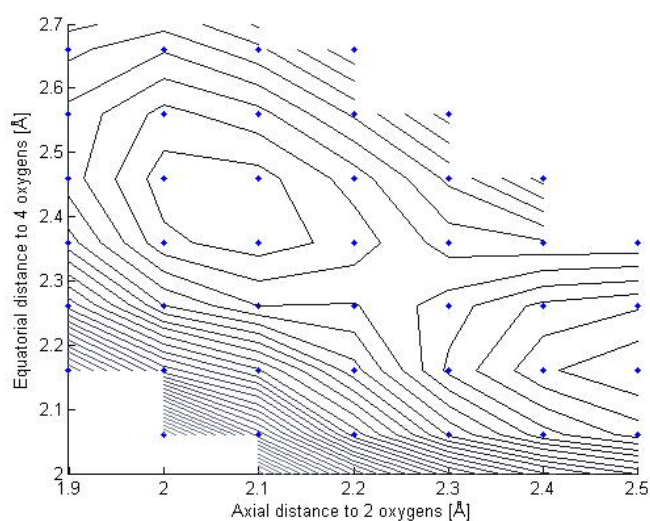


Figure 6.12: The QMSTAT energy surface of Cu^{2+} and six water molecules using the 5 states basis functions. Every contour line represents an energy difference of 0.05 eV ($k_bT = 0.026$ eV). The energy has been evaluated in the blue points and linearly interpolated between these.

Polarizable basis functions

It can be seen that for the polarizable basis function, the potential shown in figure 6.13 is generally too repulsive. The energy minima are located too far away from the ion. This can to some extent be corrected for by reducing the S2 and S6 parameters. This will however lead to poorer results for the potential curve with one water molecule and less certainty regarding the potential in other environment.

Single state basis functions

In figure 6.14 the energy curve for Cu^{2+} and six water molecules is plotted. We see that the agreement here with the CASPT2 curve is much better than

what is observed with the other potentials. Then it is also natural to believe that these basis functions will give the best results for the structure of the coordinated complex. There are, however, still some parts of the potential that are not properly described. The difference in energy between the 4+2 and 2+4 structures is only half that observed for the CASPT2 curve. If we then had observed a 4+2 structure we could be quite certain that this was the actual structure since it is disfavored in our description, however if we get a 2+4 structure it is not as easy to draw conclusions since our potential artificially favors this configuration.

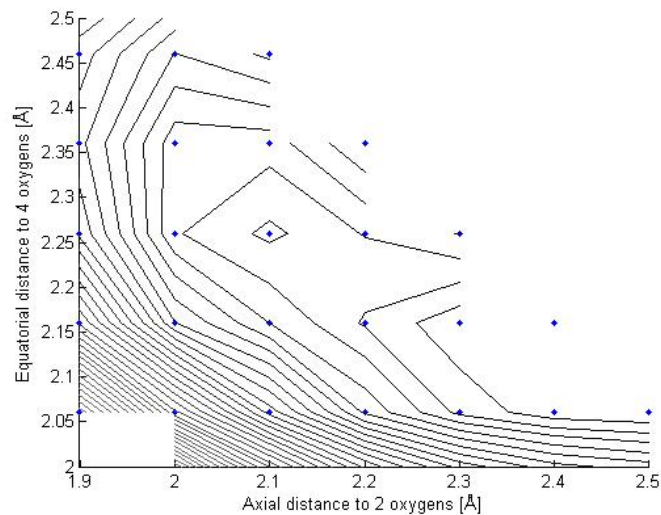


Figure 6.13: The QMSTAT energy surface of Cu^{2+} and six water molecules using the polarizable basis functions. Every contour line represents an energy difference of 0.05 eV ($k_bT = 0.026$ eV). The energy has been evaluated in the blue points and linearly interpolated between these.

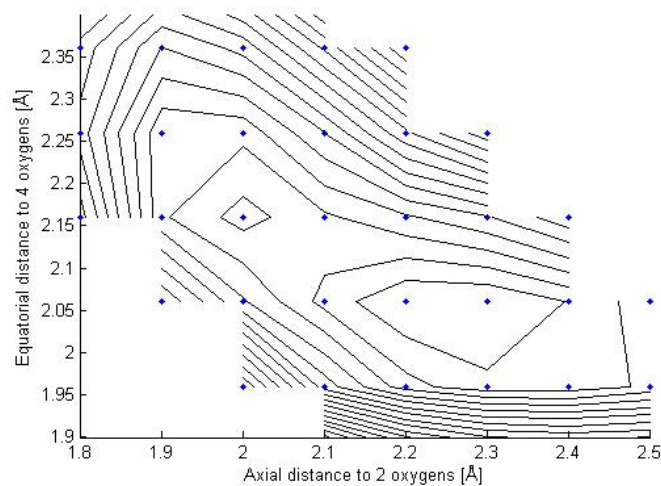


Figure 6.14: The QMSTAT energy surface of Cu^{2+} and six water molecules using the single state basis functions. Every contour line represents an energy difference of 0.05 eV ($k_bT = 0.026$ eV). The energy has been evaluated in the blue points and linearly interpolated between these.

6.3 Simulations

6.3.1 Mg^{2+} in water

The simulations with magnesium were started from three different configurations from a simulation run with copper. At the starting point the ion was pentacoordinated, but in all simulations there was a change to hexacoordination before 50,000 MC-steps had passed. The simulations were run for a total of 1,000,000 steps and no further change of configuration was found during this time for any of the simulations. The average RDF for the three simulations (MC-step 100,000 - 1,000,000) is shown in figure 6.15. A maximum in the distribution is found at 2.12 Å and the integrated curve shows that there are six waters in the first coordination shell. We also observe that the RDF drops to zero after the first coordination shell. This is because no change of coordination is observed except for the one from penta to hexacoordination which is not included when calculating the RDF. A snapshot of the structure of the water molecules around the magnesium ion is octahedral as can be seen in figure 6.16.

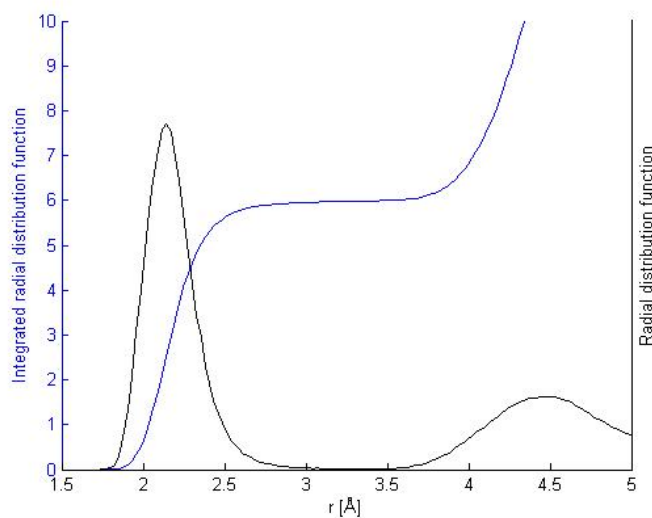


Figure 6.15: The Mg-O radial distribution function for Mg^{2+} in water taken as an average of three simulations, each lasting 900,000 MC-steps.

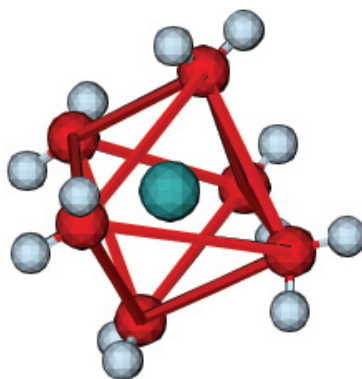


Figure 6.16: A snapshot of the first coordination shell of Mg^{2+} in water in a QMSTAT simulation. To illustrate the octahedral structure, oxygen atoms closer than 3.5 \AA from each other are connected with red bonds. The figure is made using Visual Molecular Dynamics (VMD) [68].

6.3.2 Ca^{2+} in water

Three simulations were also run with calcium, all starting from different hexacoordinated structures found in a copper simulation. Two of the simulations showed nearly identical behavior, alternating between hexa and heptacoordination, whereas the third remarked itself by having up to nine water molecules in the first coordination shell and after 1.5 million steps the polarization equations for water did not converge and the simulation aborted. The energies of the three simulations are seen in figure 6.17. It is seen here that two of the three simulations have on average the same energy, whereas the third is starting approximately 3 eV lower than the others and remains there for 600,000 MC steps before the energy starts to decrease rapidly. When the simulations were studied in detail, it was seen that the ion in parallel 2 had wandered out on the boundary of the cavity. A new simulation was started from the same starting configuration as parallel 2 where the spring constant was increased by 150 %. This time the simulation went on as the two other parallels and the Ca-ion slowly returned to origin. An increase of the spring constant will reduce the dynamics of the system but will not change the statistics as the number of MC-steps goes to infinity.

The two other simulations were run for three million steps. In figure 6.19 and 6.20 the distance to the closest water molecules in the two simulations are plotted. They are both started from a hexacoordinated configuration. Parallel 1 stays in this configuration for the first 300,000 steps before it adopts a heptacoordination and mainly remains here for the rest of the simulation, but with several instances of both eight and six water molecules in the first coordination shell. The third simulation leaves the hexacoordinated state immediately and it seems that also here is there a preference for the heptacoordinated state with some instances of a single water molecule either entering or leaving the first coordination shell. The Ca-O RDF for the two simulations that converged is shown in figure 6.18. It has a first peak with maximum at 2.50 Å which integrates to 6.9 oxygen atoms.

It is slightly disturbing that if parallel 2 had been simulated alone for 600,000 MC steps, there would not have been any signs in the energy that something was going wrong. The water coordination structure around the ion was slightly different than the two other parallels with a second coordination shell closer to the ion, but the coordination still seemed reasonable, had it been the only simulations run.

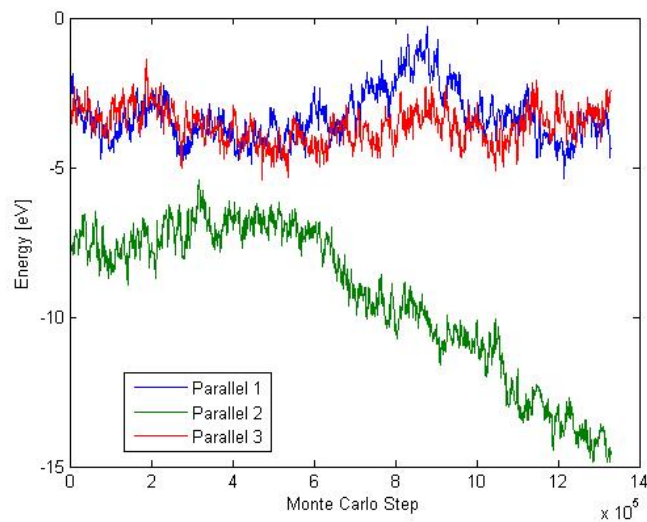


Figure 6.17: Energy for three parallel simulations of Ca^{2+} in water. Parallel 2 aborted after 1.5 million MC-steps because the polarization equations for water did not converge. It was then found that the ion had wandered out to the boundary of the cavity.

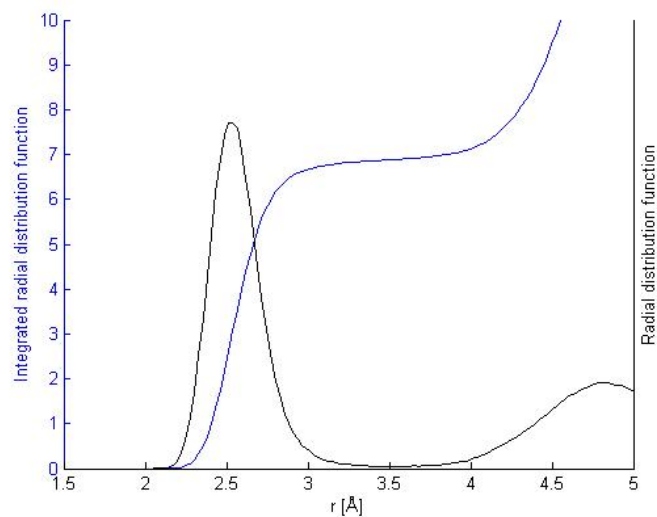


Figure 6.18: The Ca-O RDF for the simulations of Ca^{2+} in water. It is calculated as the average of two parallels (Parallel 1 and 3 in figure 6.17), each run for $3 \cdot 10^6$ MC-steps.

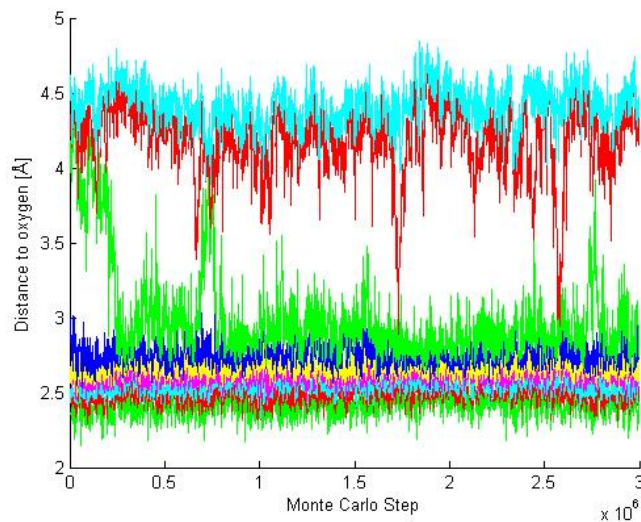


Figure 6.19: The distance from Ca^{2+} to the nine closest oxygen atoms in a QM-STAT simulation (Paralell 1 in figure 6.17) lasting $3 \cdot 10^6$ MC-steps.

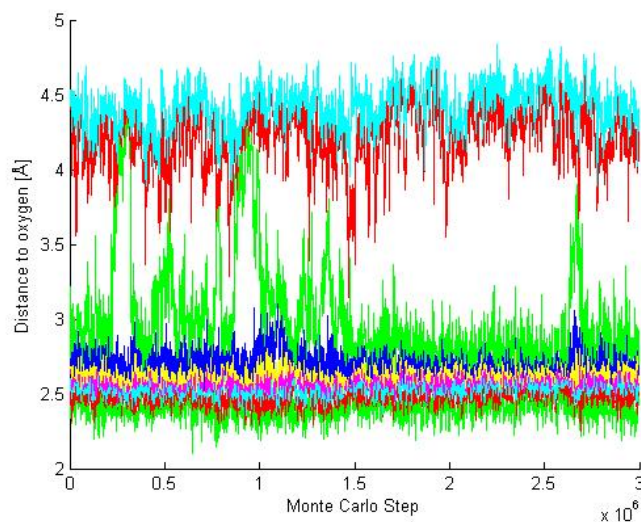


Figure 6.20: The distance from Ca^{2+} to the nine closest oxygen atoms in a QM-STAT simulation (Paralell 3 in figure 6.17) lasting $3 \cdot 10^6$ MC-steps.

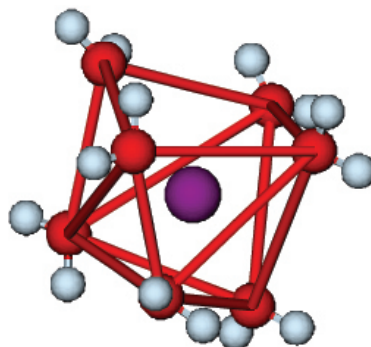


Figure 6.21: A snapshot of the first coordination shell of Ca^{2+} in water in a QMSTAT simulation. This is the heptacoordinated structure. A hexacoordinated structure was also observed similar to that for Mg^{2+} in figure 6.16. To illustrate the structure, oxygen atoms closer than 3.5 Å from each other are connected with red bonds. The figure is made using Visual Molecular Dynamics (VMD) [68].

6.3.3 Sr^{2+} in water

Three parallel simulations were performed with Sr. It was experienced that the calculations behaved strangely when run with a too large basis set. The water molecules were concentrated on one side of the ion which led to a large dipole moment in the QM-region. When the number of basis functions was reduced these problems were no longer observed and three simulations were run for 1,000,000 MC steps each. The simulations with Sr^{2+} were the most dynamical of the once performed in this work as can be seen in figure 6.22 where the closest oxygen atoms to the ions during a simulation is plotted. This is believed to be because Sr^{2+} is the softest ion does not interact as strongly with water as the other more compact and harder ions. The radial distribution function for the three simulations is shown in figure 6.23 and shows a peak at 2.60 Å, which integrated gives 8 water molecules in agreement with XD- data.

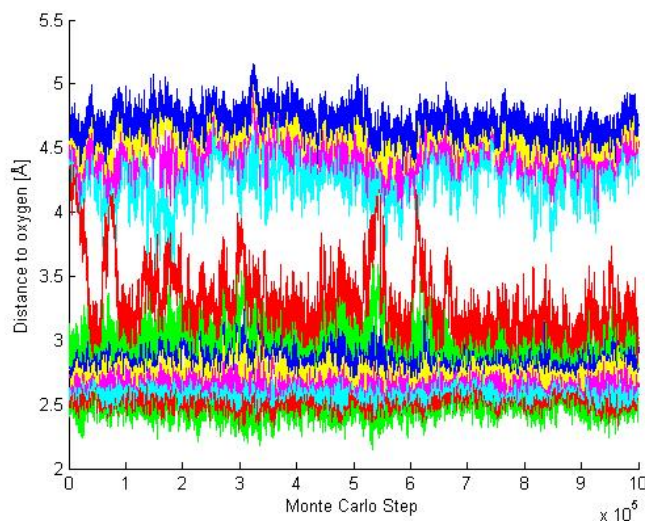


Figure 6.22: The distance from Sr^{2+} to the twelve closest oxygen atoms in a QMSTAT simulation lasting 1,000,000 MC-steps.

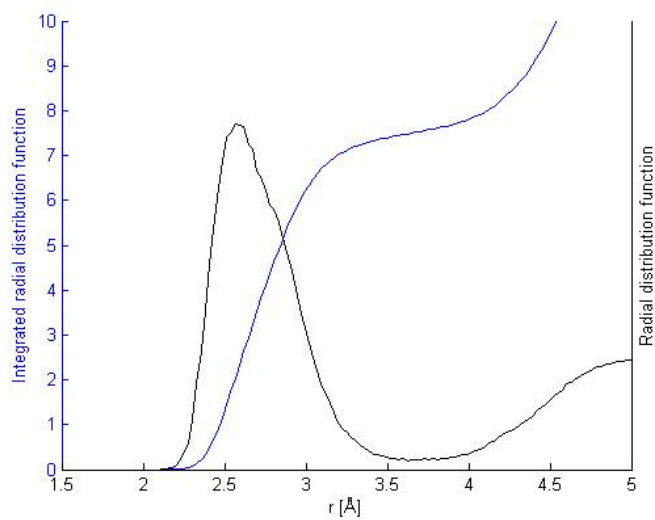


Figure 6.23: The radial distribution function from the simulations with Sr^{2+} . The distribution is taken as an average of three simulations, each lasting 1,000,000 MC-steps.

6.3.4 Cu^{2+} in water

For Cu^{2+} we had three different set of basis functions, whereof only one, the single state basis functions had the desired flexibility to be able to correctly reproduce the potential surface of copper + 1 water and copper + 6 water. Nevertheless, simulations were run also with the other potentials and the results are summarized here.

5 state basis functions For the 5 state basis function, a simulation lasting for 550,000 MC-steps was performed. During this time, both five and six water molecules were observed in the first coordination shell. It can be seen from the RDF in figure 6.24 that we have two clear peaks, the first one consisting of two water molecules at 1.96 Å and the second one at 2.45 Å containing between three and four water molecules. We also see in figure 6.25 that there is a change in coordination between five and six during the simulation and that there is a clear difference between the inner two water molecules and the next shell consisting of partly three, partly four water molecules. When we compare the results from the simulation with the supermolecular potential in figure 6.9, we see that when the ion is hexacoordinated it has a structure closely resembling the minimum energy structure with two axial oxygens at 2.05 Å and four equatorial oxygens at 2.4 Å, but since the QMSTAT-potential did not reproduce the CASPT2 potential this does not indicate that this is the true coordination structure of Cu^{2+} .

When the spectrum is estimated as described in section 5.3.2 we get the density of states shown in figure 6.26. This is in almost perfect agreement with the experimental spectrum, figure 4.1. The fact that this happens is probably that even though the description of the ground state is flawed, we observe a cancellation of errors since the first excited state is equally bad described.

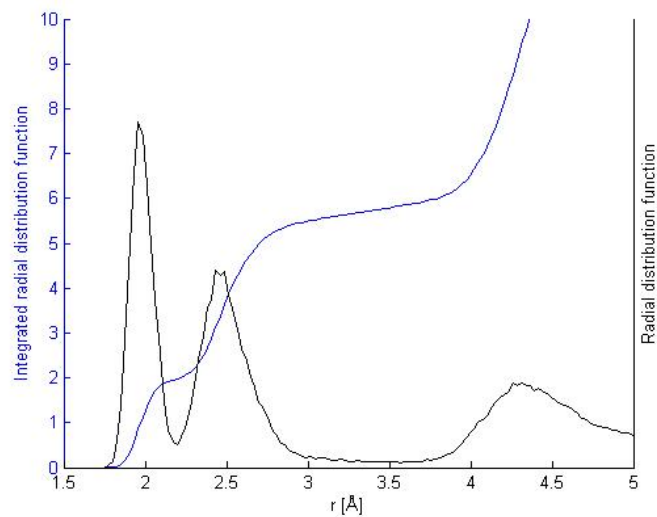


Figure 6.24: The Cu-O RDF for a QMSTAT simulation lasting for 550,000 MC-steps with the 5 states basis functions.

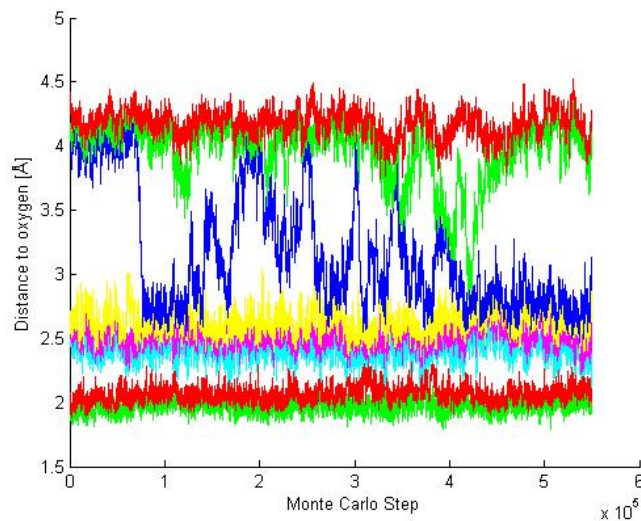


Figure 6.25: The distance from Cu^{2+} to the eight closest oxygen atoms in a QM-STAT simulation using the 5-states basis functions lasting 550,000 MC-steps.

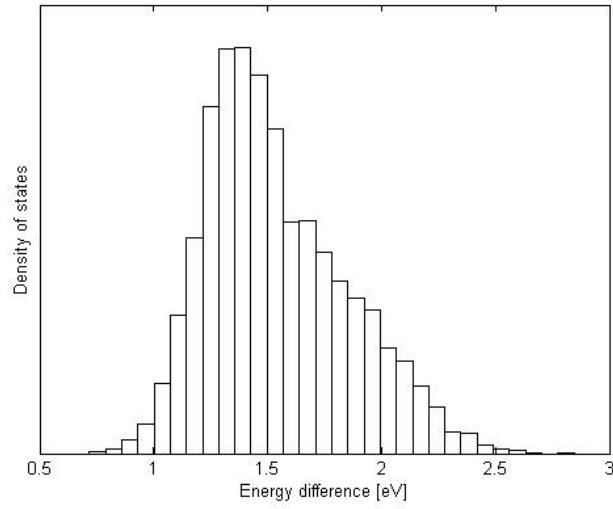


Figure 6.26: The spectrum estimated as described in section 5.3.2 with the 5-states basis functions. Taken from a simulation lasting 550,000 MC-steps.

Polarizable basis functions Three simulations were run with the polarizable basis functions, all ended up in the classical elongated octahedral structure. The radial distribution function for the average of the three simulations is shown in figure 6.27. The first peak at 2.12 Å represents four water molecules and the shoulder lying between 2.3 and 2.4 Å contains the other two. The distance to the closest oxygens is too long, previous calculations and experimental data have reported this distance to be slightly less than 2 Å and we get 2.12 Å. This is also reflected in the supermolecular potential used, shown in figure 6.13 which is too repulsive at short distances. The plot of the closest water molecules is shown for one of the parallels in figure 6.28. No change of coordination is observed during the simulation and a small gap is seen between the four innermost oxygen atoms and the succeeding two. The estimated spectrum from the simulations using the given basis is shown in figure 6.29. It is seen that it is too low in energy compared to the experimental spectrum. This might stem from the fact that the oxygens are located too far away from the ion and that the splitting of the d -orbitals because of the ligands now is less pronounced.

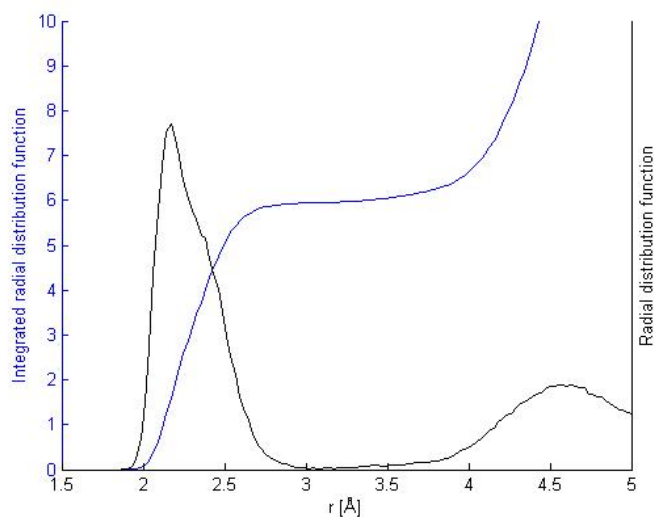


Figure 6.27: The radial distribution function with the polarizable basis functions. The distribution is taken as an average over three simulations, each lasting 500,000 MC steps.

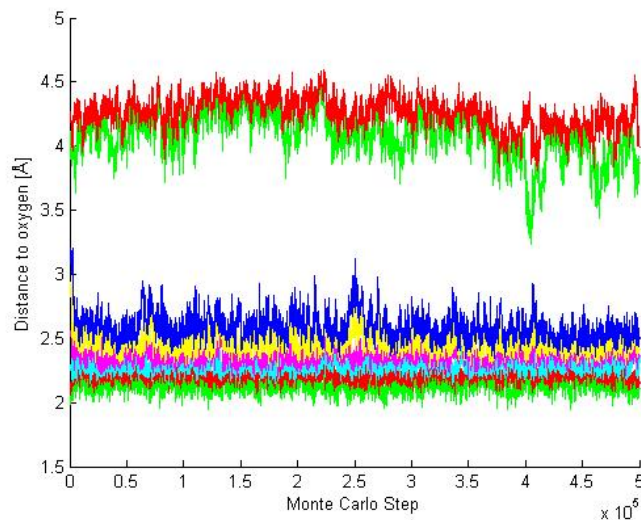


Figure 6.28: The distance from Cu^{2+} to the eight closest oxygen atoms in a QM-STAT simulation using the polarizable basis functions lasting 500,000 MC-steps.

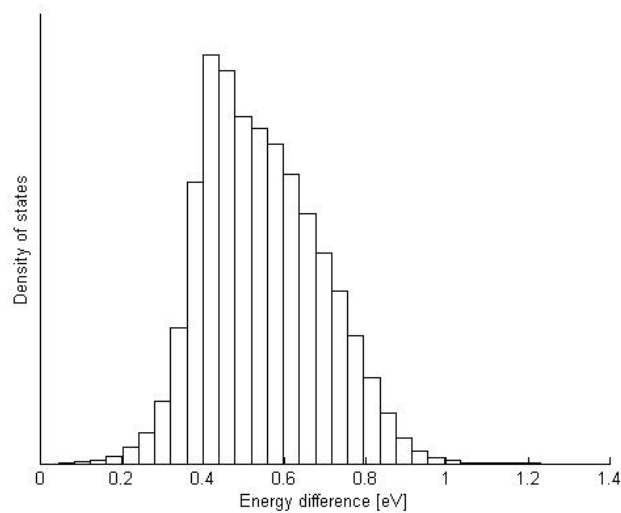


Figure 6.29: The spectrum estimated as described in section 5.3.2 with the polarizable basis functions. The spectrum is taken as an average over three simulations, each lasting 500,000 MC steps.

Single state basis functions For the single state basis functions, three simulations were run, each lasting for 600,000 MC-steps. The average radial distribution function for the three simulations is shown in figure 6.30. We see here a clear first peak at 1.96 Å and a shoulder at 2.1 -2.2 Å. From one of the simulations a plot of the eight closest water molecules is shown in figure 6.31. As seen there is no change in coordination during this simulation, but there are many transitions where there occur change in coordination between the compressed and the elongated octahedral structure. Which water molecules that are included in the innermost peak in the radial distribution function, are also constantly changing.

In the QMSTAT potential pictured in figure 6.14 the lowest minimum is for the elongated octahedron in accordance with the classical picture of Cu^{2+} . However, during the simulations it is often observed that the coordination takes the form of a compressed octahedron. To investigate whether this shift in structure occurred because of effects from the second coordination shell or whether the effect was entropic in nature, we also ran a simulation with only six water molecules present for 200,000 MC-steps. The structure then found is shown in figure 6.34. It is seen here that two water molecules are clearly nearer the positive ion than the four others. This effect was much more pronounced when running the simulation with only six water molecules than with 100 water molecules. The entropic stabilization is also larger in the case where only six water molecules are present, since the rotational freedom for water molecules further from the core here is larger than if a second coordination shell is present.

The estimated spectrum from these simulations is given in figure 6.32. We see that the energy is red-shifted significantly compared to the experimental absorption spectrum, figure 4.1. This is likely to be because our description of the excited states is insufficient.

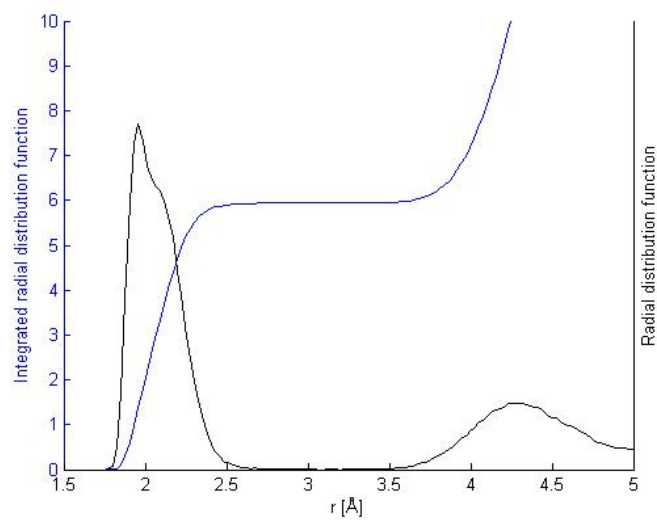


Figure 6.30: The radial distribution function from the simulation with Cu^{2+} using the single state basis functions. The distribution is taken as an average of three simulations, each lasting 600,000 MC-steps.

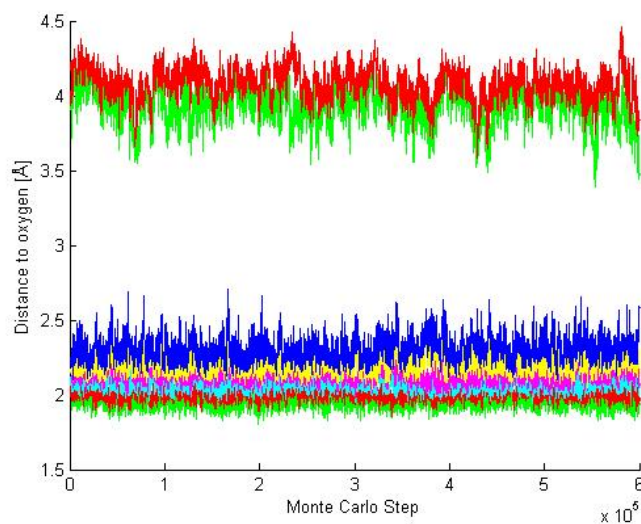


Figure 6.31: The distance from Cu^{2+} to the eight closest oxygen atoms in a QM-STAT simulation using the single state basis functions lasting 600,000 MC-steps.

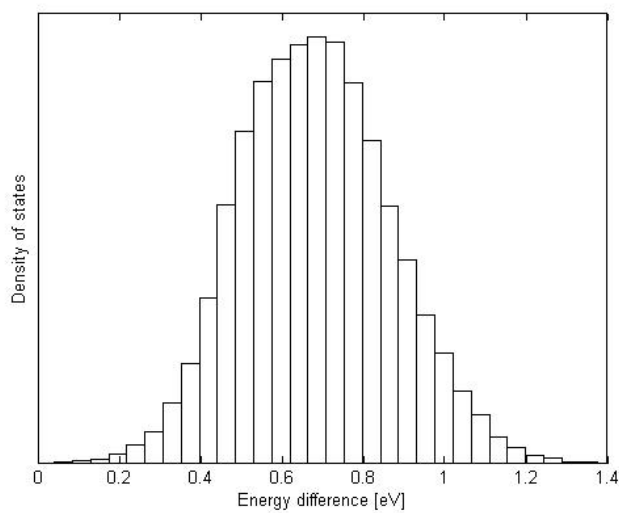


Figure 6.32: The spectrum estimated as described in section 5.3.2 with the Single state basis functions. The spectrum is estimated from an average of three simulations, each lasting 600,000 MC-steps.

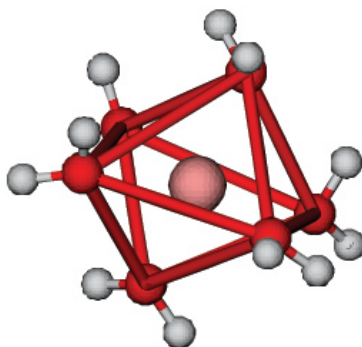


Figure 6.33: A snapshot of the first coordination shell of Cu^{2+} in water in a QMSTAT simulation using the single state basis function. The structure here is hexacoordinated, slightly compressed. To illustrate the structure, oxygen atoms closer than 3.5 Å from each other are connected with red bonds. The figure is made using Visual Molecular Dynamics (VMD) [68].

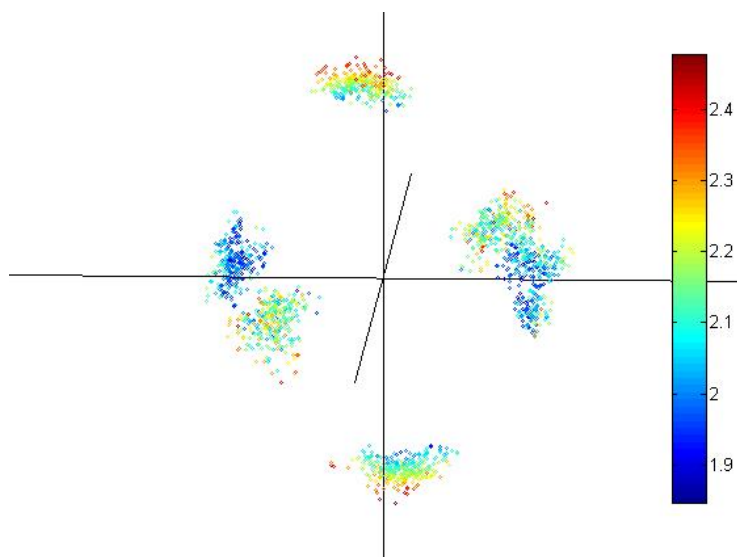


Figure 6.34: Simulation run with only six water molecule and a Cu^{2+} ion. The dots are the location of the oxygens relative to the ion taken in every 100th MC-step over a total of 30,000 MC-steps. The color is the distance from origin [\AA]. It can clearly be seen that two of the water molecules are located closer (bluer) than the other four.

Chapter 7

Discussion

7.1 Quality of the results

For the four simulated ions we get results for both the coordination number and the ion oxygen distance that are in agreement with previously reported experimental and theoretical work, but since no absolute consensus regarding the coordination structure of the ions exists, it is still hard to state what the correct answer should look like. What can be said, is that the models used for the ions and the ion- water interaction in these simulations are based solely on quantum mechanical data and are able to reproduce energy curves from supermolecular calculations. In addition the simulations are run long enough to observe several changes in coordination for the ions, which would indicate that the statistics has converged. This combined makes the QMSTAT approach promising for determining coordination structures. The cost in computational resources is an order of magnitude less than for QM/MM simulations.

7.2 The coordination of Mg^{2+}

For magnesium experiments, QM/MM and MD simulations seems to agree on a six-coordinated structure. This is also the smallest ion with the least electronic flexibility of the ones we have studied, and thus where the polarization of the ion plays the least important role and where MD simulations with water polarizability would be expected to give reasonable results. In our simulations we also get a six-coordination with the first peak in the RDF at 2.12 Å. This is in agreement with ND data (2.10 Å) and QM/MM simulations (2.12 Å). Because of the hard structure of the ion it is commonly believed that it is well described by the ground state and the choice of basis functions will thus not heavily influence the results.

7.3 The coordination of Ca^{2+}

There is more dispute over the coordination structure of calcium than over that of magnesium. ND experiments have reported from 6 to 10 water molecules in the first coordination shell and the first peak in the RDF from 2.39 - 2.46 Å. QM/MM simulations report a CN between 7.6 and 8.3 with a shortest distance between 2.45 and 2.50 Å. In the QMSTAT simulations we observe 2.50 Å with between 6 and 8 water molecules in the first coordination shell. One reason for the dispute on coordination number is naturally that there is no definite CN, but it fluctuates in time. This is consistent with our results and the fact that we see more changes of coordination structure with calcium than for any of the other ions.

7.4 The coordination of Sr^{2+}

For Sr^{2+} we get a structure with eight water molecules in the first coordination shell, but where short transitions occurs with either seven or nine water molecules occurs. The first peak in our RDF is located at 2.60 Å. This is in agreement with the scarce experimental data that shows a octocoordination with the first peak in the RDF at 2.62 Å.

7.5 The coordination of Cu^{2+}

The ion is commonly believed to be hexacoordinated with an elongated octahedral structure. We also find in supermolecular CASPT2 calculations that this is the minimum energy structure consistent with previous results with CISD calculations of the ion and six water molecules. On the other hand, we find that when we used a potential with the elongated octahedral as the minimum energy structure (the single state basis functions), and run a simulation using only six water molecules, we end up in *compressed* octahedral structure. This illustrates an important point. The energy difference between different minima can in coordination chemistry in some cases be small enough to let entropic effects push the complex from the global energy minimum structure to another *free* energy minimum. The four water molecules close to the ion have less rotational and translational freedom and this makes the structure with only two water molecules at short distances entropically favored.

When simulations are run, using the same potential and 100 water molecules, we observe dominantly the classical elongated octahedral structure, where the water molecules that are closest to Cu^{2+} are constantly changing and where transition structures that are in the compressed octahedral structure are observed.

It is seen from the CASPT2 calculations on Cu^{2+} (figure 6.5) that the energy valley that governs the transition between an elongated and compressed octahedron is shallow and broad with an energy difference between the two minima

of approximately 1% of the total water ion interaction energy. This may explain the fluctuating results from ND experiments. In a elongated structure with the four closest oxygens at 1.96 Å, the two more distant waters may move between 2.2 and 2.5 Å, almost without changing the complex' energy. The complex structure will then be very dependent on other ions in the system and the exact experimental conditions, leading to differing results found by different experimentalists.

7.6 The absorption spectrum of Cu^{2+}

The spectrum for copper as we estimate it is approximately 0.5 eV too low in energy compared to the experimental spectrum in figure 4.1. Since the ground states structure seems to give a good description of the energy surface found using CASPT2, it seems likely that our description of the excited states is inadequate. One possible way to calculate the spectrum is to take some structures obtained during the simulations and calculate the energy of the few first excited states in these configurations. This has not been done in this work, but would be a natural way to check whether the configurations found are plausible or not. Including all water molecules in a Quantum Mechanical calculation may be too computationally expensive, but two shells of water on the CASSCF level should be possible at the present level.

7.7 The QMSTAT approach

7.7.1 Partly covalent character

In the physical world there is no strict barrier between intramolecular and intermolecular interactions. In the QMSTAT model, on the other hand, the system is divided into molecules and the interactions within these groups are of one kind, whereas the interaction between these groups is modeled in another way. The most critical example of where this description fails to include all effects is the interaction between the central ion and the closest water molecules. There is a double positive charge on a relative small ion and the electrons of water will have a tendency to be transferred to the ion. The electron is no longer completely located on water and a covalent bond will start to form. This is seen in the supermolecular quantum mechanical calculations where a significant transfer of charge, from the surrounding water molecules to the ion. This effect is not only caused by the forming of a covalent bond, but is also caused by Basis Set Superposition Error, BSSE. Since we use a finite basis set for our molecules, the water molecules would have been able to reduce their energy by using the ionic orbitals, also without the positive charge located there. We correct for the energy in this interaction with the counterpoise method but we do not have a measure of how much electronic density on the ion is caused by the BSSE.

7.7.2 The electric interaction

It is seen from the interaction potentials between water and a dipositive ion that the potential in QMSTAT is not as attractive as the one calculated using MP2. One possible reason for this is the parameterization of the NEMO water model. When this modeled was developed the SCF dipole moment was used to determine the charges on the atomic centers and the polarizability [37]. The dipole moment in an SCF calculation is higher and the polrizability lower in a SCF calculation than when including electron correlation. A cancellation of error occurs in pure water such that the properties of water are still correctly described. However, when we introduce a positive charge in the system, it may be that in this strong electric field the lower SCF polarizability causes the net dipole moment of water to be smaller than what it would have been in an MP2 treatment.

7.7.3 The multipole expansion

Another issue that might lead the discrepancy between the QMSTAT electric interactions is the multicenter multipole expansion. When a water oxygen is approaching a positive cation, it will feel less and less of the negative electric charge from the electron cloud it as enters the electron cloud of the ion. The effect is in reality a higher positive net charge and more attraction. In the QM-STAT model however, this is not accounted for more than in a dipole expansion of the central ion. A model incorporating these effects would have to calculate the overlap integral over the charge distributions. This would be feasible but would require a large revision of the QMSTAT code, but it is seen as an important step on the way for future development of QMSTAT.

The missing charge transfer term, the low polarizability and the multipole expansion of the charges will all make the interaction energy between water and a positive ion too low. To compensate for this the exchange repulsion has to be reduced to reproduce the supermolecular potential. This can again lead to problems with the supermolecular potentials and when reproducing the spectra it will lead to a smaller change in energy between the ground state and the first excited state since the difference in energy between these is mostly due to exchange interaction and not much influenced from electrostatic interactions. This means that this can be an important reason why the calculation of the spectra fails for Cu.

7.7.4 Polarization catastrophes

Polarization catastrophes were obeserved for the simulations with Ca and Mg. They were both characterized by a slow wandering of the QM-ion out on the border of the cavity over approximately 1 million MC steps. This happened even though the ion was anchored to the center of the cavity with a spring potential on the form

$$U_{spring} = k_{spring} r_{Ion}^2, \quad (7.1)$$

with r_{Ion} being the distance from origin to the ion and the spring constant chosen to be 0.002 Hartree/Bohr² (0.194 eV/Å²). The reason for this is believed to be the high interaction energy between a charge and a dielectric medium. The ion is attracted to the border of the cavity and moves here. At the border the description of the QM-region is to some degree unphysical because of the discontinuity there. The water molecules are repelled from the dielectric medium whereas the QM-region is not. It is seen that one of the water molecules is squeezed against the discontinuity and the polarization catastrophe happens when the distance between the QM-region and the water molecule becomes too short. It was seen that when increasing the spring constant to 0.005 Hartree/Bohr² the QM-region held its position in the center of the cavity with the same starting configurations as the ones where a catastrophe were observed. An increased constant will not influence the sampling in the limit where the number of MC steps goes toward infinity, but will make the dynamics of the system slower.

7.7.5 The explicit solvent model

It is common practice when simulating molecules or ions in water to include the interaction with water as the effect of a dielectric continuum. Such a description naturally has its weaknesses. Especially when there are strong electric forces in the system as for charged species and where hydrogen bonds are present. Such bonds will act between two explicit molecules and can not be correctly treated if not the model incorporate them as such. The NEMO water model in QMSTAT is a clear improvement from continuum models and includes explicit water molecules in a way that allow quantum mechanical treatment of the central molecule, together with an explicit model for the surrounding media in a way that still allows longer simulations to be performed.

7.7.6 The length of the simulations

When comparing the length of these simulations with ones using MD or DFT, one must naturally regard that no time exists in a MC simulation. If the simulation goes through transition states it is possible to make an estimate of the time extension by comparing how many times a given energy barrier has been broken in the MC simulations and compare to how frequent such breakages are using MD.

In a QM/MM simulation running for 14 ps, 4 occurrences was seen of water molecules either entering or leaving the first coordination shell of Ca²⁺ [52]. In the QMSTAT simulations with Ca²⁺ we observed twice in simulations run for 3,000,000 MC-steps, 6 such changes. This means that 1,000,000 MC-steps roughly corresponds to 7 ps of simulation, but such estimates should be used with great care and are not very reliable. Also in the mentioned QM/MM

simulation an equilibrium structure was found with a mean Ca-O distance of 2.60 Å, significantly more than in other simulations and experiments. This could also imply that the complex is artificially labile and the estimated exchange rate too high, which again means that the estimated time of the QMSTAT simulation, is too low.

Chapter 8

Conclusion

It is seen that the QMSTAT approach shows promise when describing the coordination structure also for divalent ions. For all the four ions investigated, we get coordination structures that are within the uncertainty limits of what has been observed with both experimental and computational methods previously. We also get insight into the dynamic coordination structure of the ions. Compared to average values obtainable using experimental methods, we have a much better time resolution and compared to the short simulation times obtained using QM/MM simulations, QMSTAT have the possibility to obtain true converged statistics.

The coordination structure of Cu^{2+} is observed to be governed by the exact shape of a broad valley in the energy surface. To predict with certainty the coordination structure of this ion, will require a precise description of this energy landscape, more exact than what is achieved using QMSTAT. It has been shown in this report that entropic effects also play a major role for the structure of this first coordination shell.

Acknowledgments

I would like to thank prof. Gunnar Karlström for his great hospitality and many interesting discussions. Anders Öhrn has been of great help, answering an endless row of questions and sharing his vast knowledge with me. I would also like to thank my supervisor in Trondheim, prof. Per Olof Åstrand for helpful comments. And in the end, a warm thanks to Hannah Rosquist who made my stay in Lund outstanding.

Bibliography

- [1] Vinogradov, E. V.; Smirnov, P. R.; Trostin, V. N. *Rus. Chem. Bull. (Int. Ed.)* **2003**, *52*, 1253 - 1271.
- [2] Rohde, B. M.; Hofer, T. S. *Pure Appl. Chem.* **2006**, *78*, 525-539.
- [3] Bernath, F. *Phys. Chem. Chem. Phys.* **2002**, *4*, 1501-1509.
- [4] Zumdahl, S. S. *Chemistry*; Houghton Mifflin: Boston, Mass., 4th ed.; 1997.
- [5] Berg, J. M.; Stryer, L.; Tymoczko, J. L. *Biochemistry*; W. H. Freeman & Co.: Madison Avenue, New York 10010, 5th ed.; 2002.
- [6] Öhrn, A.; Karlström, G. *Mol. Phys.* In press.
- [7] Ohtaki, H.; Radnai, T. *Chem. Rev.* **1993**, *93*, 1157-1204.
- [8] Salmon, P. S.; Neilson, G. W.; Enderby, J. E. *J. Phys. C: Solid State Phys.* **1988**, *21*, 1335-1349.
- [9] Marcus, Y. *Chem. Rev.* **1988**, *88*, 1475-1498.
- [10] Lee, P. A.; Citrin, P. H.; Eisenberger, P.; Kincaid, B. M. *Rev. Mod. Phys.* **1981**, *53*, 769 - 806.
- [11] Atkins, P. W.; Friedman, R. S. *Molecular Quantum Mechanics*; Oxford University Press: New York, 3rd ed.; 1997.
- [12] Jahn, H. A.; Teller, E. *Proc. Roy. Soc. A* **1937**, *161*, 220-235.
- [13] Siesler, H. W.; Ozaki, Y.; Kawata, S.; Heise, H., Eds.; *Near-Infrared Spectroscopy*; Wiley-VCH: Weinheim, 1st ed.; 2002.
- [14] Dirac, P. A. M. *Proc. Roy. Soc. A* **1928**, *610*, 117.
- [15] Schrödinger, E. *Ann. Phys.* **1926**, *384*, 489-527.
- [16] Griffiths, D. J. *Introduction to Quantum Mechanics*; Prentice Hall: New Jersey, 2nd ed.; 2004.
- [17] Born, M.; Oppenheimer, R. *Ann. Phys.* **1927**, *389*, 457-489.
- [18] Singh, U. C.; Kollman, P. A. *J. Comp. Chem.* **1986**, *7*, 718-730.
- [19] Boys, S. F. *Proc. Roy. Soc. A* **1950**, *200*, 542-554.

-
- [20] Leach, A. R. *Molecular Modeling principles and applications*; Pearson Education Limited, England: Second ed.; 2001.
- [21] Metropolis, N.; Rusembluth, A. W.; Rusembluth, M. N.; Teller, A.; Teller, E. *J. Chem. Phys.* **1953**, *21*, 1087-1092.
- [22] Christen, M.; Hünenberger, P. H.; Bakowies, D.; Baron, R.; Bürgi, R.; Geerge, D. P.; Heinz, T. N.; Kastenholz, M. A.; Kräutler, V.; Oostenbrink, C.; Peter, C.; Trzesniak, D.; van Gunsteren, W. F. *J. Comp. Chem.* **2005**, *26*, 1719-1751.
- [23] Swope, W. C.; Andersen, H. C.; Berens, P. H.; Wilson, K. R. *J. Chem. Phys.* **1982**, *76*, 637-649.
- [24] Berendsen, H. J. C.; Postma, J. P. M.; van Gunsteren, W. F.; DiNola, A.; Haak, J. *J. Chem. Phys.* **1984**, *81*, 3684-3690.
- [25] Nosé, S. *J. Chem. Phys.* **1984**, *81*, 511-519.
- [26] Sherwood, P. . In *Modern Methods and Algorithms of Quantum Chemistry*; Grotendorst, J., Ed.; John von Neumann Institute for Computing: 2000; Chapter Hybrid quantum mechanics/molecular mechanics approaches, pages 257-277.
- [27] Mordasini, T.; Thiel, W. *Chimia* **1998**, *52*, 288-291.
- [28] Nachtigallova, D.; Nachtigall, P.; Sierka, M.; Sauer, J. *Phys. Chem. Chem. Phys.* **1999**, *1*, 2019-2026.
- [29] Karlström, G.; Lindh, R.; Malmqvist, P.-Å.; Roos, B. O.; Ryde, U.; Veryazov, V.; Widmark, P.-O.; Cossi, M.; Schimmelpfennig, B.; Neogrady, P.; Seijo, L. *Comp. Mat. Sci.* **2003**, *28*, 222-239.
- [30] Lindh, R.; Ryu, U.; Liu, B. *J. Chem. Phys.* **1991**, *95*, 5889-5897.
- [31] Weisstein, E. W. "Hermite-Gauss Quadrature", From MathWorld—A Wolfram Web Resource. <http://mathworld.wolfram.com/Hermite-GaussQuadrature.html>.
- [32] Roos, B. O.; Taylor, P. R.; Siegbahn, P. E. M. *Chem. Phys.* **1980**, *48*, 157-173.
- [33] Malmqvist, P.-Å.; Rendell, A.; Roos, B. O. *J. Phys. Chem.* **1990**, *94*, 5477-5482.
- [34] Malmqvist, P.-Å.; Roos, B. O. *Chem. Phys. Lett.* **1989**, *155*, 189-194.
- [35] Møller, C.; Plesset, M. S. *Phys. Rev.* **1934**, *46*, 618-622.
- [36] Andersson, K.; Malmqvist, P.-Å.; Roos, B. O. *J. Chem. Phys.* **1992**, *96*, 1218-1226.
- [37] Wallqvist, A.; Ahlström, P.; Karlström, G. *J. Phys. Chem.* **1990**, *94*, 1649-1656.
- [38] Friedman, H. L. *Mol. Phys.* **1975**, *29*, 1533-1543.

- [39] Margenau, H.; Kestner, N. R. *Theory of Intermolecular Forces*; Pergamon Press Ltd.: Headington Hill Hall, Oxford, 1st ed.; 1969.
- [40] Öhrn, A.; Karlström, G. *J. Phys. Chem. B* **2004**, *108*, 8452-8459.
- [41] Öhrn, A.; Karlström, G. *J. Phys. Chem. A* **2006**, *110*, 1934-1942.
- [42] Bock, C. W.; Kaufman, A.; Glusker, J. P. *Inorg. Chem.* **1994**, *22*, 419-427.
- [43] Adrian-Scotto, M.; Vasileva, D.; Mallett, G.; Vasilescu, D. *Internet Electron. J. Mol. Des.* **2004**, *3*, 400-411.
- [44] Matwiyoff, N. M.; Taube, H. *J. Am. Chem. Soc.* **1968**, *90*, 2796-2800.
- [45] Neilson, G. W.; Tromp, R. H. *Annu. Rep. Phys. Chem. C* **1991**, *88*, 45-75.
- [46] Pye, C. C.; Rudolph, W. W. *J. Phys. Chem. A* **1998**, *102*, 9933-9943.
- [47] Tongraar, A.; Rode, B. M. *Chem. Phys. Lett.* **2001**, *346*, 485-491.
- [48] Probst, M. M.; Radnai, T.; Heinzinger, K.; Bobb, P.; Rode, B. M. *J. Phys. Chem.* **1985**, *89*, 753-759.
- [49] Hewish, N. A.; Neilson, G. W.; Enderby, J. E. *Nature* **1982**, *297*, 138-139.
- [50] Jalilehvand, F.; Spongberg, D.; Lindqvist-Reis, P.; Hermanson, K.; Person, I.; Sandstrom, M. *J. Am. Chem. Soc.* **2001**, *123*, 431-441.
- [51] Bakó, I.; Hutter, J.; Pálinkás, G. *J. Chem. Phys.* **2002**, *117*, 9838-9843.
- [52] Naor, M. M.; Nostrand, K. V.; Dellago, C. *Chem. Phys. Lett.* **2003**, *369*, 159-164.
- [53] Albright, J. N. *J. Chem. Phys.* **1972**, *56*, 3783-3786.
- [54] Caminiti, R. *J. Appl. Cryst.* **1982**, *15*, 482-487.
- [55] Seward, T. M.; Henderson, C. M. B.; Charnock, J. M.; Driesner, T. *Geochim. Cosmochim. Acta* **1999**, *63*, 2409-2418.
- [56] Tanaka, K.; Johansen, H. *Int. J. Quant. Chem.* **1997**, *64*, 453-458.
- [57] Salmon, P. S.; Neilson, G. W. *J. Phys.: Condens. Matter* **1988**, *1*, 5291-5295.
- [58] Becke, A. D. *J. Chem. Phys.* **1993**, *98*, 5648-5652.
- [59] Lee, C.; Yang, W.; Parr, R. G. *Phys. Rev. B* **1988**, *37*, 785-789.
- [60] Pasquarello, A.; Petri, I.; Salmon, P. S.; Parisel, O.; Car, R.; Tóth, .; Powell, H.; Fischer, H. E.; Helm, L.; Merbach, A. E. *Science* **2001**, *291*, 856-859.
- [61] Rode, B.; Schwenk, C.; Hofer, T.; Randolf, B. *Coord. Chem. Rev.* **2005**, *249*, 2993-3006.
- [62] Shivaiah, V.; Das, S. K. *Ang. Chemie* **2006**, *45*, 245-248.

- [63] Richens, D. T. *The Chemistry of Aqua Ions*; Wiley: Chichester, UK, 1st ed.; 1997.
- [64] Boys, S. F.; Bernardi, F. *Mol. Phys.* **1970**, *19*, 553-566.
- [65] Pierloot, K.; Dumez, B.; Widmark, P.-O.; Roos, B. O. *Theor. Chim. Acta* **1995**, *90*, 87-114.
- [66] Roos, B. O.; Veryazov, V.; Widmark, P.-O. *Theor. Chim. Acta* **2003**, *111*, 345-351.
- [67] Douglas, M.; Kroll, N. M. *Ann. Phys.* **1973**, *82*, 89-155.
- [68] Humphrey, W.; Dalke, A.; Schulten, K. *J. Mol. Graph.* **1996**, *14*, 33-38.